Polymer Electrolyte Electrolysis: A Review of the Activity and Stability of Non-Precious Metal Hydrogen Evolution Reaction and Oxygen Evolution Reaction Catalysts

Hughes, J.P.[1,2], Clipsham, J.[3], Chavushoglu, H.[1,2], Rowley-Neale, S.J.[1,2*] and Banks, C.E.[1,2*]

[1]: Faculty of Science and Engineering, Manchester Metropolitan University, Chester Street, Manchester M1 5GD, UK.

[2]: Manchester Fuel Cell Innovation Centre, Manchester Metropolitan University, Chester Street, Manchester M1 5GD, UK.

[3]: European Marine Energy Centre, The Charles Clouston Building, ORIC, Back Rd, Orkney KW16 3AW, UK

*To whom correspondence should be addressed.

Email: c.banks@mmu.ac.uk; Tel: ++(0)1612471196; Fax: ++(0)1612476831

Website: www.craigbanksresearch.com

Abstract

The potential for generating green hydrogen by electrolysis (water splitting) has resulted in a substantial amount of literature focusing on lowering the current production cost of hydrogen. A significant contributor to this high cost is the requirement for precious metals (namely Pt and Ir/Ru (oxides)) to catalyse the two main reactions involved in electrolysis: the hydrogen evolution reaction (HER) and the oxygen evolution reaction (OER). Herein we overview the current literature of non-precious metal HER and OER catalysts capable of efficient water splitting within a polymer electrolyte membrane (PEM) electrolyser, recording the activity and stability of each catalyst and allowing for direct comparison to be made. Additionally, we highlight the inapplicability of catalyst stability testing in many academic studies for commercial electrolyser applications and propose a universal stability-testing regime for HER and OER catalysts that more accurately mimics the conditions within an operating electrolyser.

Highlights

- Stability studies of cathodic catalysts don't translate to commercial electrolysis
- Anodic catalyst stability studies are more comprehensive for electrolysis operation
- Stability of novel catalysts needs to be benchmarked against the optimal catalysts
- Combining active and stable first row transition metals shows promising catalysis
- A stability testing regime for proton exchange membrane electrolysis is proposed

Word count:

Keywords: Energy storage; PEM Electrolyser; hydrogen evolution reaction; renewable energy, oxygen evolution reaction; water splitting.

LIST OF ABBREVIATIONS

A-Ni-C: Activated-Ni-Carbon

ATO: Antimony Tin Oxide

AWS: Alkaline Water Electrolysis

BPP: Bipolar Plate

CCM: Catalyst Coated Membrane

CD: Current Distributor

Co-N-GA: Cobalt Embedded Nitrogen Graphene Aerogel

Cu: Copper

DFT: Density Functional Theory

ECSA: Electrochemically Active Surface Area

Fe: Iron

Fe_2P: Iron (II) Phosphide

Fe_3P: Iron (III) Phosphide

FeP: Iron Phosphide

GO: Graphene Oxide

H_2: Hydrogen

HCl: Hydrochloric Acid

HER: Hydrogen Evolution Reaction

HET: Heterogeneous Electron Transfer

$Ir(O_2)$: Iridium (oxide)

LGDL: Liquid Gas Diffusion Layer

Li: Lithium

MEA: Membrane Electrode Assembly

Mn: Manganese

MOF: Metal Organic Framework

MoS_2: Molybdenum Disulfide

NHE: Normal Hydrogen Electrode

Ni: Nickel

NPM: Non-Precious Metal

O_2: Oxygen

OER: Oxygen Evolution Reaction

OWS: Overall Water Splitting

O_x: Oxide

Pb: Lead

PEM: Proton Exchange Membrane or Polymer Electrolyte Membrane

Pt: Platinum

rGO: Reduced Graphene Oxide

RHE: Reversible Hydrogen Electrode

$Ru(O_2)$: Ruthenium (oxide)

Sb: Antimony

SOE: Solid Oxide Electrolysis

Ta: Tantalum

Ti: Titanium

TMC: Transition Metal Chalcogenide

TMD: Transition Metal Dichalcogenide

TMP: Transition Metal Phosphide

V: Vanadium

1. Introduction

Green hydrogen gas is a promising vector for the storage and transportation of the energy generated from renewable sources due to its high energy density (140 MJ/kg), which exceeds that of current fuels, such as; coal (24 MJ/kg) and petrol (44 MJ/kg).[1] Hydrogen is mainly utilised in the chemical industry, where global production currently stands at 500 billion cubic meters (bm^3) per annum.[2] Hydrogen can be produced by a variety of techniques such as natural gas reformation, coal or biomass gasification and electrolytic processes.[3] The generation of hydrogen *via* water splitting, within an electrolyser, is considered the "greenest" hydrogen production technique, as it does not produce any direct carbon emissions when powered by renewable sources such as wave, wind and solar.[4-8]

Electrolytic water splitting devices are categorized dependent upon their operating conditions, the most common variants being:[7, 8]

- Alkaline water electrolysis (AWS) is electrolysis within an alkaline electrolyte using a diaphragm to separate product gases and to transport hydroxide ions (OH^-). AWS typically operates at temperatures of 5-100°C[9], operating pressures of 25-30 bar, achieving current densities of up to 400 mA/cm^2 and energy efficiencies up to 40%.[9-11]
- Solid oxide electrolysers (SOE) use a solid oxide or ceramic electrolyte to generate hydrogen with a steam feedstock. SOE operate at high temperature (500-850°C), pressures of more than 50 bar, achieving current densities of more than 3 A cm^{-2} and energy efficiencies up to 50%.[12, 13]
- Polymer electrolyte membrane (PEM) electrolysis occurs within an acidic electrolyte using a proton exchange membrane to transport protons (H^+). PEM electrolysis operates at temperatures of 50-80°C, pressures of less than 30 bar, achieving current densities of above 2 A cm^{-2} and energy efficiencies of 50-65%.[14]

PEM electrolysis is the most promising electrolytic method for producing green hydrogen due to its high-energy efficiencies comparable to AWS and SOE. The achievable current densities in SOE are the highest of the water splitting devices; however, SOE is limited by poor catalyst stability and membrane degradation, given the nature of its operating conditions.[15, 16] PEM electrolysis allows for the generation of high purity hydrogen (up to 99.999 vol. %)[17-19] at high-pressures, which reduces the requirement for post-production gas compression.[20-22] For the reasons

highlighted above, the generation of hydrogen *via* PEM electrolysis is the most attractive technology for commercial applications. Note that whilst we acknowledge the presence of other essential components within a PEM electrolyser (*i.e.* gas diffusion layer, flow plates, etc) this manuscript solely focuses on anodic and cathodic catalyst materials for PEM electrolysis in acidic conditions.

Electrolytic water splitting within a PEM electrolyser is made up of two half reactions (under standard conditions):

The anodic reaction (oxidation) is the oxygen evolution reaction (OER):

Eq.1 $$2H_2O\ (l) \rightarrow O_2\ (g) + 4H^+\ (aq) + 4e^-$$ $E^o = +\ 1.23$ V (*vs.* RHE)

and the cathodic reaction (reduction) is the hydrogen evolution reaction (HER):

Eq.2 $$2H^+(aq) + 2e^- \rightarrow H_2(g)$$ $E^o = 0.00$ V (*vs.* RHE)

where the overall water splitting (OWS) reaction is:

Eq.3 $$2H_2O\ (l) \rightarrow 2H_2\ (g) + O_2\ (g)\ (\mathrm{OWS})$$ $E^o = +\ 1.23$ V (*vs.* RHE)

Any additional energy input over + 1.23 V that is required in order to induce water splitting is known as the overpotential (η) and represents the intrinsic thermodynamic inefficiency of a particular system.[23] The HER has a negligible activation energy whilst the OER has a large kinetic inhibition (large η) originating from a 4-electron proton coupled mechanism, as described by *Eq.1*.[24, 25] Hence, the development of effective OER electrocatalysts is critical given that the OER is the limiting factor to an electrolyser's efficiency.[26]

Only 4% of the global production of hydrogen is *via* electrolysis,[27-29] this is due to an absence of financial incentives to invest in "green" hydrogen energy from renewables, given that it is considerably more expensive than its fossil fuel counterparts to produce. For example, the cost to produce 1kg of hydrogen using grid electricity is currently £11.40,[30] whereas, the cost to produce 1 gallon of diesel is £4.47. In automotive terms, 1kg of hydrogen is roughly equivalent in mileage to 1 gallon of diesel.[31] The above costs include capital and operating expenses. The high cost associated with hydrogen generation *via* PEM electrolysis is partly due to the expensive components utilized, such as the membrane electrode assembly (MEA), which accounts for 24% of the overall electrolyser cost.[28] The MEA contains low earth abundant precious metals, namely

Pt and Ir, that are required to efficiently catalyse the HER and OER.[32-35] It is important to note that the price of pure Pt metal has increased from £10.58 to £28.23 per gram in the last 20 years.[36] Similarly, the price of pure Ir metal has increased from £11.11 to £58.22 per gram in the last 20 years.[37] The trend of increasing price of Pt and Ir is set to continue over the coming years, as more resources are used up.[38] Hydrogen produced utilising electrolyser technologies containing these precious metals will likely experience a corresponding price increase. The transition from precious to non-precious metal (NPM) based catalyst layers within the MEA is therefore key to reducing the overall cost of PEM electrolyser technologies, however, achieving suitable stability of these materials in an acidic electrolyte remains a challenge.[39, 40]

Given the aim of reducing the cost of hydrogen production *via* PEM electrolysis, researchers have attempted to produce NPM catalysts capable of efficient water splitting. In order for NPMs to have the potential of replacing precious metal catalysts, within a commercial electrolyser, they need to exhibit low overpotentials towards the HER or the OER and achieve high current densities in acidic conditions. Enhancing the lifetime of the PEM cell and stack is critical to commercial implementation; therefore, the catalyst materials must also show excellent stability and corrosion resistance in acidic media. This paper will provide a detailed overview of the currently available literature regarding NPM catalysts for use as the cathodic and anodic materials within PEM electrolysers.

2. *Overview of the Activity and Stability of HER Electrocatalysts*

Presently, platinum (Pt) or Pt based electrocatalysts exhibit optimal electrochemical activity towards the hydrogen evolution reaction (HER), however long term application within commercial electrolysers is limited by high cost and low earth abundance.[41-53] Below we present an overview of NPM cathodic catalysts that exhibit excellent activity towards the HER. The potential for scalability within NPM catalysts is dependent on the loading of the catalyst material, where a higher mass loading may reach a plateau with precious metal catalysts in regards to activity, but would result in inflated overhead and material costs. The activity per unit mass (or mass activity) is therefore a critical metric to assessing a NPM catalysts feasibility for use within commercial PEM electrolysis.[54] Typical loading of commercial Pt/C on the cathode of a PEM electrolyser is 0.5–1.0 $mg_{Pt}\,cm^{-2}$, where the mass activity of Pt/C is *ca.* 0.27 A mg^{-1} at 50 mV (*vs.* RHE).[55-57] The stability of each HER catalyst in acidic conditions will be discussed and referenced to the benchmark stability of Pt/C, which remains stable for 50 hours during chronopotentiometry measurements at − 10 mA cm^{-2}.[58] Note, that a commercial PEM electrolyser has been quoted to exhibit a lifetime of up to 60000 h with no decay in cell voltage.[59, 60] The outlook regarding the decline in PEM electrolyser performance is currently focused on catalyst degradation at the anode, however these degradation mechanisms are poorly understood.[60, 61] Brightman and co-workers[62] have demonstrated that changes in the electrochemically active surface area (ECSA) and degradation of the Pt cathode results from power cycling in a PEM electrolyser, which is thought to have a more significant effect on the performance of a PEM electrolyser than initially thought. Thus, it is critical that studies of HER catalysts include extensive stability reports. Within this study we are addressing ways in which laboratory scale electrochemical techniques can assess the suitability of a catalyst for commercial PEM electrolysis. ESI Table 1 outlines the current optimal HER electrocatalysts, with Figure 1 displaying the HER onset potential (*V vs.* RHE) *vs.* current density at − 150mV (mA cm^{-2}) for the catalysts highlighted within this table. The HER onset is determined as the potential at which the Faradaic current commences, which is signified by the observed current deviating from the background current by the value of − 25 μA cm^{-2}.[63]

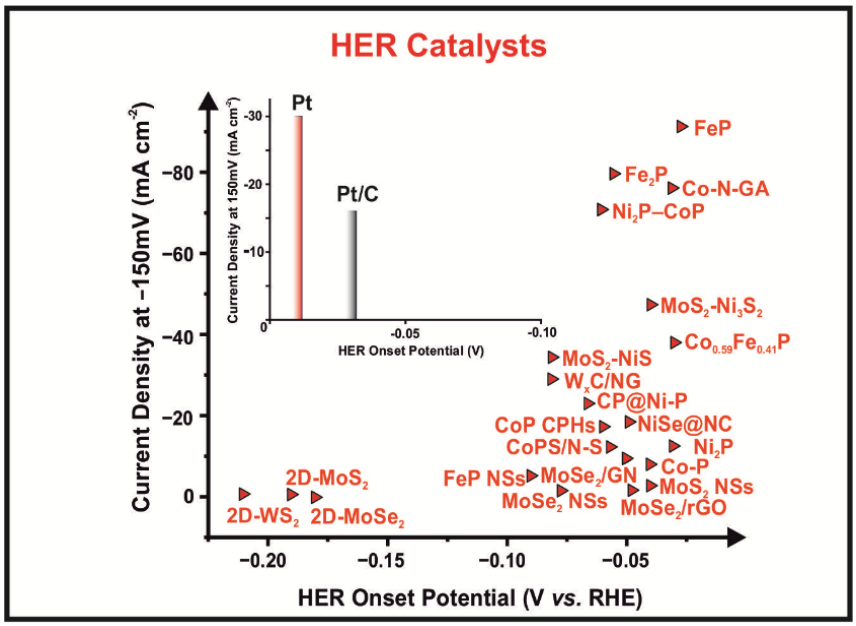

Figure 1 Graphical overview of optimal performing catalysts towards the hydrogen evolution reaction (HER) in acidic media; HER onset potential (V *vs.* RHE) against the current density (mA cm^{-2}). Note that the current density is the value taken at − 150 mV as is common within literature. Inset exhibits the optimal HER activity of Pt and Pt/C for comparison

2.1 Transition metal dichalcogenides (TMD's)

In recent years, transition metal dichalcogenides (TMD's) such as MoS_2,[42, 64] $MoSe_2$,[44, 65] WS_2[66, 67] and WSe_2[44, 68] have been shown to be promising cathodic materials to act as HER catalysts. A TMD nanosheet consists of two layers of chalcogens surrounding a single plane of a transition metal, where multiple layers are bonded by out-of-plane Van Der Waals interactions.[53] TMD's contain two anisotropic planes: the relatively inert basal planes, and the highly active edge planes, which exhibit a fast rate of heterogeneous electron transfer (HET).[69] An example of the use of a TMD towards the HER is a study by Wang *et al.*[70] who electrochemically tuned 2H-MoS_2 with Li *via* a lithiation reaction, with sulfonated MoS_2 (S-MoS_2) conducting Li electrochemical intercalation. This resulted in a layer exfoliation and 2H to + 1T phase conversion (semi conducting to metallic). Li-MoS_2 was chemically deposited onto carbon fibre paper and exhibited a HER onset potential of *ca.* − 0.10 V (*vs.* RHE). For comparison, the optimal polycrystalline Pt electrode exhibits a HER onset potential of − 0.01 V (*vs.* RHE).[71] The 1T phase of MoS_2 possesses a larger number of active sites compared to the 2H phase, which results in a higher charge transfer rate. Due to the metallic character in the partially filled d-band the 1T phase

is *10^7 times more conductive* than the 2H phase.[72] Increasing the ECSA of the electrode by reducing the size of the deposited nanoparticles also enhances conductivity and allows for stronger interactions. The 1T phase of Li-MoS_2 exhibits high achievable current densities of − 200 mA cm^{-2} at η= 200 mV; and exhibits a mass activity of 0.20 A mg^{-1} at 0.1 V (*vs.* RHE), which is nearing the mass activity of commercial Pt/C (0.27 A mg^{-1} at 0.05 V (*vs.* RHE*)*).[73, 74] However, there is insufficient stability data to conclude the suitability of the material within a PEM electrolyser. A small potential window between + 0.1 to − 0.2 V (*vs.* RHE) was used to assess the variance in HER onset potential over 7000 cycles. This is not representative of the measured cell voltage of an operating PEM cell using benchmark Pt/C and Ir catalyst materials, which can be between + 1.4 and + 2.0 V.[75] When assessing catalysts, the complete potential range of a PEM electrolyser must be taken into account. This is due to the process of passivity, where corrosion of the catalyst layers during periods of electrolyser inactivity, or during cell operation, can lead to oxidative conditions within the cathodic catalyst layer.[76] Wang and co-workers[70] carried out potentiostatic measurements at a η= 118 mV (*vs.* RHE) which reflected little variation in the current density (*ca.* − 10 mA cm^{-2}) over a 2 hour duration. The duration of this stability measurement is too short when compared against the benchmark stability of the Pt/C catalyst, which remains stable for more than 50 hours within the same conditions. Additionally, PEM electrolysers quote a stack lifetime of between 20000-60000 hours,[77] therefore more information must be provided regarding the stability of this HER catalyst.

The HER catalysis of TMD's can also be optimised by hybridisation with a graphitic material such as graphene and carbon nanotubes. Introducing graphitic additives is a method of increasing the number of electronic conductive pathways and therefore the conductivity of a material.[78] Doping TMD's with transition metals increases electron density at the electrocatalytic active sites, and thus facilitates electron transfer at the edge planes.[79] Guo *et al.*[80] enhanced the catalysis and conductivity of MoS_2 with Vanadium and Nitrogen dopants and reduced graphene oxide (rGO), respectively: V, N-MoS_2/rGO. The V, N-MoS_2/rGO composite was synthesized *via* a solvothermal method, which increased the number of defect sites on the basal and edge planes. A HER onset potential of − 0.03 V (*vs.* RHE) was reported by the V, N-MoS_2/rGO suggesting excellent HER kinetics. The V, N-MoS_2/rGO also displays a high achievable current density of − 100 mA cm^{-2} at an overpotential of *ca.* 160 mV, however there is no statement of mass activity, hence there is no defining activity metric to assess whether the V, N-MoS_2/rGO is a feasible cathodic alternative

to commercial Pt/C within a PEM electrolyser. Note that previous reports have stated the mass activity of MoS_2/rGO to be 0.085 A mg^{-1} at 0.1 V (*vs.* RHE)[81, 82] Chronoamperometric measurements at η= 90 mV (*vs.* RHE) for 20h exhibits no variation in a current density of − 20 mA cm^{-2}. The absence of any long-term stability data involving TMD's is likely a result of their instability within aqueous solutions, over a large pH range. The suitability of any MoS_2 containing materials for PEM electrolysis is highly unlikely given the formation of oxidative defects, in the form of MoO_3, on the surface of MoS_2 nanosheets when in the presence of water.[83]

It is also common to hybridise $MoSe_2$ with graphene additives.[84, 85] Certain studies have highlighted that $MoSe_2$ expresses the smallest band gap of all TMD's and therefore exhibits the best conductivity, where direct bandgaps of 1.88, 1.57, 2.03 and 1.67 eV relate to MoS_2, $MoSe_2$, WS_2 and WSe_2.[86] Tang *et al.*[87] hydrothermally prepared $MoSe_2$ nanosheets and $MoSe_2$/rGO which exhibited HER onset potentials of − 0.15 and − 0.05 V (*vs.* RHE), respectively. The HER onset potential exhibited by the $MoSe_2$/rGO hybrid is stated as an improvement on its MoS_2 counterpart, where a comparative study displays a HER onset potential of − 0.08 V (*vs.* RHE) for its MoS_2/rGO hybrid.[82] Additionally, the previously reported values of 0.085 and 0.14 A g^{-1} for the mass activity of MoS_2/rGO and $MoSe_2$/rGO at 0.1 V (*vs.* RHE) demonstrates that $MoSe_2$ exhibits superior HER catalysis (*Note: the mass activity of $MoSe_2$ is still not competitive with commercial Pt/C*).[88, 89] This is explained by density functional theory (DFT) calculations for Gibbs free energy for hydrogen absorption (ΔG^0_H) at different H^+ surface coverages on each TMD nanosheet. A proficient HER catalyst such as Pt will exhibit a ΔG^0_H value close to the thermoneutral value ($\Delta G^0_H = 0$).[90] Values of − 0.14 and − 0.23 eV, are expressed by $MoSe_2$ at 75% H^+ surface coverage and MoS_2 at 50% H^+ surface coverage, respectively. Note that the values of ΔG^0_H for $MoSe_2$ and MoS_2 stated within this study were those that were closest to the thermoneutral value. Tang and coworkers probed the stability of their $MoSe_2$/rGO catalyst deposited on fluorine doped tin oxide (FTO) using chronoamperometry measurements at 200 mV, where a slight degradation in current density from *ca.* 13.0 to *ca.* 12.5 mA cm^{-2} was observed over a 2 hour duration. It should be noted that displaying a catalyst stability study for a duration of 2 hours is not sufficient to conclude that a catalyst displays efficient HER catalysis. Therefore, it is not appropriate to conclude that the $MoSe_2$/rGO catalyst utilised within this study is applicable to commercial PEM electrolysis given that the benchmark Pt/C catalyst remains stable for up to 50 hours.[91]

2.2 Metal organic framework derivatives

Metal organic frameworks (MOF's) are typically organic/inorganic porous materials composed of grouped or ungrouped metal centres bound to organic ligands to exhibit a crystalline morphology.[92] The HER catalysis displayed by MOF's is determined by a number of factors. The highly porous nature of MOF's results in surface roughness and therefore a high number of exposed active sites and enhanced heterogeneous electron transfer (HET). The HET process occurs at the triple phase boundary, which comprises of the electrolyte, catalyst phases and gaseous species within a PEM electrolyser.[93] Porosity also results in a large ECSA, which allows for the significant interface between the electrolyte and catalyst surface. Surface porosity plays a significant role in the nature of hydrogen adsorption and desorption, where stronger proton adsorption leads to a faster supply of protons, but can also lead to slow release of hydrogen from active sites, hence poor HER kinetics. The porosity of MOF's may be tuned to achieve balanced adsorption/desorption behaviours. The nature of adsorption and desorption is dependent on the interaction between unfilled *d* orbitals of the transition metal and *s* orbitals of hydrogen.[94] MOF's possess compositional flexibility, where the transition metal *d* orbitals can be tuned to increase electron density and enhance the HER activity.[95] Pristine MOF's often suffer from poor conductivity and high charge transfer resistance. This can be mitigated by anchoring MOF's to carbon supports, which can significantly improve catalytic activity by increasing the number of electron conductive pathways.[96, 97] Zhu *et al.*[98] developed a cobalt embedded nitrogen graphene aerogel (Co-N-GA) whilst they controlled the porosity by confining the growth of MOF's within the graphene aerogel. The Co-N-GA exhibits excellent catalysis towards the HER with a HER onset potential of *ca.* − 0.03 (*vs.* RHE), nearly matching the activity of Pt/C. The graphene aerogel and pristine MOF exhibit negligible HER activity, suggesting that the excellent performance of Co-N-GA is a result of the Co embedded in the few layered N-doped carbon aerogel. The optimized porosity of the Co-N-GA achieved by etching and hydrothermal treatment also contributed to the excellent HER catalysis. The Co-N-GA displays good achievable current density, reaching − 100 mA cm^{-2} at η= 183 mV. The suitability of Co-N-GA within PEM electrolysers relies on its mass activity and stability within acidic media. The mass activity of the Co-N-GA is not reported within the study and there is no data within the literature regarding a comparable HER catalyst within acidic media. This metric should be considered in future studies

utilising this catalyst. Promising stability data is offered within the study where chronoamperometry at − 0.11 V (*vs.* RHE) does not alter the current density at − 45 mA cm^{-2}. However, there is no evidence of the Co-N-GA's corrosion resistance over a longer duration than 5000s. Given that the HER activity of this catalyst is benchmarked against Pt/C, the stability must also be referenced to Pt/C. The absence of long-term stability data is likely a result of the instability of the GA component in acidic conditions, as literature suggests that graphene degrades with prolonged exposure to water, and low pH conditions.[99-101]

Isolated metal atoms (Ni, Fe and Co) have previously demonstrated proficient electrochemical activity towards the HER, due to their low coordination and unsaturated atoms functioning as active sites.[102] Fan *et al.*[103] developed an activated-Ni-carbon (A-Ni-C) catalyst, by carbonising an Ni-MOF precursor at 700°C to obtain Ni@C, where HCl leaching was repeated to dissolve exposed Ni metal. A constant potential was applied to activate the catalysts (shown in Figure 2(A)). The A-Ni-C catalyst displays a HER onset potential of − 0.03 V (*vs.* RHE) and achieves a current density of − 100 mA cm^{-2} at η= 112 mV as shown in Figure 2(B). There is no data on the mass activity of the A-Ni-C, however Xue *et al.*[104] anchored zero valence single Ni atoms on graphdiyne which exhibited a mass activity of 16.6 A mg^{-1} at 0.2 V (*vs.* RHE), which is 7.19 times higher than Pt/C (2.31 A mg^{-1}). The excellent catalysis and conductivity of the A-Ni-C is attributed to the synergistic electrical charge transfer between catalytic active sites and the underlying graphitic carbon. Figure 2(C) displays a HAADF STEM image of A-Ni-C where atomically isolated Ni species (marked by white circles) are dispersed on the partially graphitized carbon support, with 78% of the Ni species being isolated as single atoms. Figure 2(D) shows constant-potential activation at η= 200 mV to drive hydrogen bubble production upon the surface of A-Ni–C modified GC electrodes. Chronoamperometric measurements at η = 45 mV revealed fluctuating current deviation during 25 hour measurements. The current density undergoes an increase at 11 hours to *ca.* − 14 mA cm^{-2}, which is due to catalyst activation. Consequently, the stability of the active catalyst is only tested for 14 hours. The absence of a long-term stability study is likely a result of the instability of metallic Ni in acidic conditions. Ni undergoes very fast dissolution in weakly acidic solutions when exposed to normal operating temperatures of a PEM cell. In the temperature range 65-75°C, full nickel dissolution is likely achieved in less than 200 minutes.[105] The thermal and acidic instability of single atom Ni make it unsuitable for cathodic application within a PEM electrolyser. Similarly, Co and Fe dissolve in 0.5 M H_2SO_4 under thermal and

potential control, however, corrosion of these metal atoms may be inhibited by alloying with metal ions such as Zn^{2+} and Mn^{2+}.[106, 107] The dissolution of metal ions in acidic conditions is inhibited by the strong adsorption of Zn^{2+} and Mn^{2+} onto the primary metal surface, the primary metals being Ni, Co or Fe. When Zn^{2+} and Mn^{2+} are deposited onto the surface of the primary metal, they increase the potential at which dissolution occurs, because they exhibit less electronegative HER onset potentials compared to Ni, Co or Fe. This method is called under potential deposition, and has beneficial effects on the stability of a catalyst, however leads to the increase in onset potential of the HER and OER.[108]

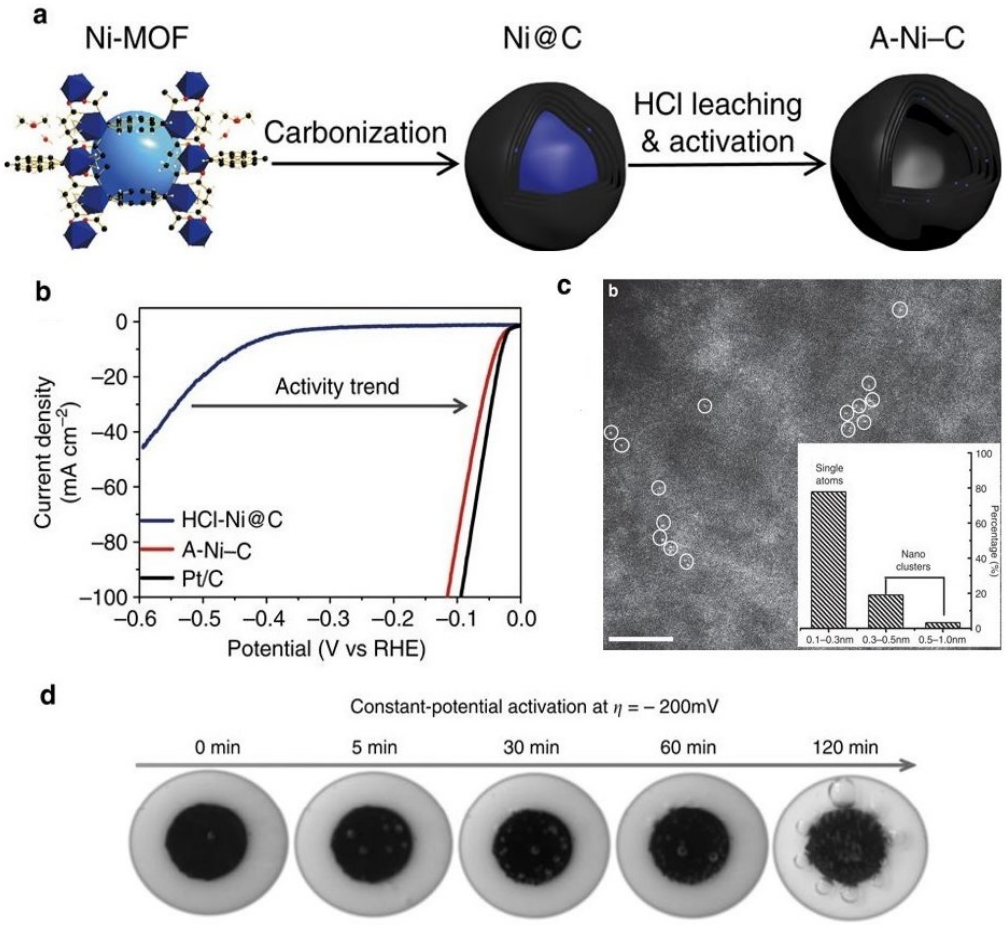

Figure 2 (A) Schematic diagram of synthesis and activation process of the Ni–C catalysts. **(B)** LSV curves of HCl-Ni@C, A-Ni–C and Pt/C in 0.5 M H_2SO_4 **(C)** Subångström resolution HAADF STEM image of A-Ni–C. The circles are drawn around isolated Ni atoms. Scale bar, 3 nm. Inset of b; the size distribution figure, which is based on >120 observed Ni species counted from high-magnification images (recorded at 4 × original magnification). (**D)** Hydrogen bubbles driven at η= 100 mV at GC electrodes postactivation (potential activation at η= 200 mV for

different times: 0, 5, 30, 60 and 120 mins). All the digital photos were taken when the cell was supplied η= 100 mV for 20 s. Adapted with permission from ref.[103]

2.3 Transition metal phosphides (TMP's)

The study of transition metal phosphides (TMP's) as active and stable cathodic materials has led to interesting discoveries about the nature of catalysis within transition metals and the electro kinetic contribution of phosphide ions. First row transition metals typically follow the trend of Mn < Fe < Co < Ni in regards to their electrochemical performance towards the HER; however, the trend is reversed when we consider the stability of the monometallic ion in acidic media.[109] The phase space of TMP's has brought attention to their performance as catalysts for the HER, given that variation of phase and crystal structure of the transition metal results in different properties. For example iron phosphides, FeP, Fe_2P and Fe_3P all exhibit different catalytic activity and stability in acidic media.[110] The crystal systems of FeP, Fe_2P and Fe_3P are orthorhombic, hexagonal and tetragonal, respectively.[111-113] Fe_3P is made up of the weakest covalent bonds in the ferric species but exhibits the strongest ionic interactions, largest metallicity and contains the largest number of Fe-Fe interactions. Exposed stepped surfaces of 3-fold Fe and Fe-Fe bridge sites are thought to exhibit affinity for H^+ ions, where Fe-P sites result in weaker adsorption of H^+ ions.[114] Similarly to the iron phosphides, Ni-Ni interactions are responsible for strong hydrogen absorption, whereas Ni-P interactions exhibit weaker H^+ affinity. An increase in the transition metal content leads to pronounced *d*-band character across the fermi level,[115] which results in advantageous adsorption/desorption behaviours, larger areas of electron density and a higher number of active sites within the compound.[116] Moon *et al.*[117] demonstrated that the Ni_2P crystal is made up of two types of Ni and P site, denoted in Figure 3(A) as Ni (I), Ni (II), P (I) and P (II). Figure 3(B) exhibits two types of supercell models. The first model displays exposed Ni_3P_2 upon the (0 0 1) surface and the second exposed Ni_3P upon the (0 0 2) surface. The density of state (DOS) for the supercell models of Ni_2P informs us how developed the *d*-band is across the fermi level, where a higher DOS relates to significant adsorbent interaction, hence a lower activation barrier for the HER. The DOS of each Ni_2P surface is exhibited in Figure 3(C) where the (0 0 1) surface is closer to the fermi level. The Ni_2P synthesized by the ligand stabilization method exhibits excellent electrochemical performance towards the HER with a HER onset potential of − 0.03 V (*vs.* RHE), which is comparable to the HER onset potential of the optimal Pt/C electrocatalyst. The HER activity of Ni_2P remains unchanged after 500 cycles (Shown in Figure 3(D)). Cyclic

voltammetry (CV) is repeated over a number of cycles to evaluate whether the onset potential has diminished over the course of repeat Faradaic processes. The onset potentials of catalysts are typically assessed by CV up to 10,000 cycles,[118-120] therefore, 500 CV cycles is not sufficient to assess the longevity of a catalysts onset potential. The corrosion resistance and stability of the Ni_2P catalyst is not displayed within the study with no chronopotentiometric data to assess long-term durability. Transition metals alloyed with P show reduced metal dissolution in acidic media, as it is less thermodynamically favoured. Ni_2P with a phosphorus content of ~30% P exhibits excellent corrosion resistance, making it more suitable as a cathodic catalyst layer within a PEM electrolyser; whereas, phosphorus content of ~15% P in a TMP is unsuitable, as stability and PEM cell lifetime would be reduced.[76] However, higher P content can also lead to the restriction of electron delocalization in the transition metal, hence reducing the conductivity and the HER catalysis.[121]

Wang *et al.*[122] electrodeposited NiP on carbon fibre paper (CP) which displayed an overpotential of 18 mV in 0.5 M H_2SO_4. The CP@Ni-P remained stable after 150 hours of chronopotentiometry at − 10 mA cm^{-2} in acidic conditions. XPS conducted before and after the stability measurement showed that, the major phase of the CP@Ni-P catalyst was Ni_5P_4 with minor contributions from Ni_2P and NiP_2. This is a prime example of how a higher P content can lead to excellent durability. It is also an example of how X-ray photoelectron spectroscopy (XPS) can be used to analyse the composition of samples after long duration stability testing, where major phases responsible for specific properties, such as stability, may be quantified. This information can then be used to further tune the properties of a catalyst. Note: the mass activity data regarding the use of TMP's towards the HER in acidic conditions is sparse and inconsistent within the literature, in terms of the potential at which the mass activity is determined, therefore is not representative of TMP's this reported manuscript.[123-125]

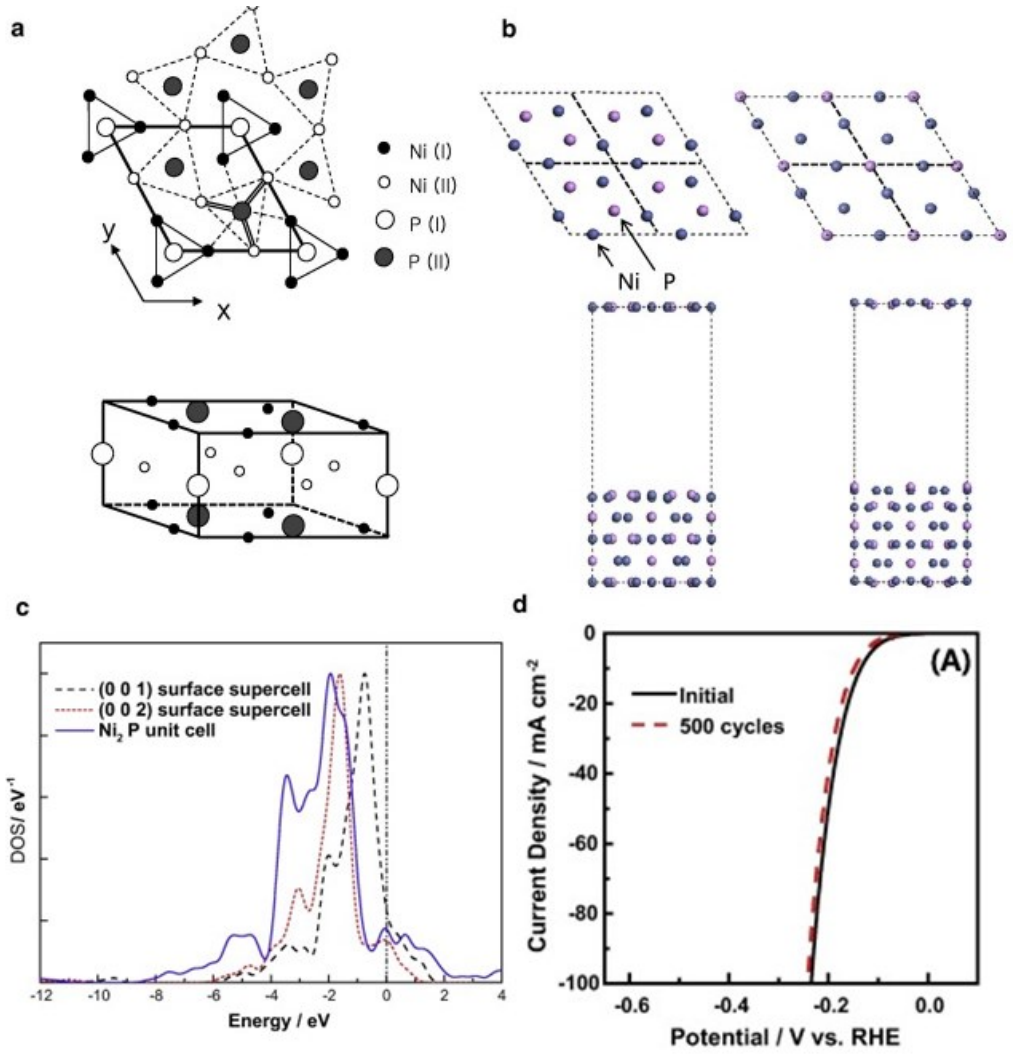

Figure 3 (A) Unit cell of Ni_2P **(B)** supercell models of Ni_2P (0 0 1) and (0 0 2) surfaces **(C)** Calculated density of state (DOS) of Ni_2P unit cell and Ni_2P supercell exposed both (0 0 1) and (0 0 2) surface. (**D)** Polarization curves of the HER before and after the acceleration durability test (ADT) for 500 cycles. All measurements were carried out in 0.5 M H_2SO_4 at room temperature and compensated for an ohmic loss. Adapted with permission from ref.[117]

3. Overview of the Activity and Stability of OER Electrocatalysts

Electrolytic water splitting is limited by the slow kinetics of the 4-electron coupled mechanism of the OER (shown in *Eq.1*) and therefore requires an efficient catalyst, which typically comprises of Ir and Ru oxides.[32, 126, 127] In recent years, there has been a lot of research highlighting the excellent performance of OER catalysts in alkaline conditions, however these catalysts tend to be highly unstable in an acidic environment. The anchoring of OER catalysts to carbonaceous supports, as is common within HER studies, is not applicable for research of anodic catalysts within PEM electrolysers, where high oxidation potentials lead to the formation of oxide films at the anode and corrosion of carbon materials..[128-131]

This section will focus on anodic NPMs that exhibit low OER onset potentials and high achievable current densities. The majority of studies do not include the crucial activity metric of mass activity, however where possible the mass activity of specific NPM OER catalysts will be compared against that of IrO_2 (*ca.* 0.30 A g^{-1} at 1.52 V (*vs.* RHE)).[132, 133] The acidic environment (pH 0-3) created by the sulfonated Nafion™ membrane within a PEM cell demands the use of corrosion-resistant catalysts, therefore the OER materials will be evaluated based on their stability within acidic conditions. Stability testing regimes for precious metal containing OER catalysts such as IrO_2, have included chronopotentiometry measurements of up to 200 h, where the catalyst remains stable at a current density of 28 mA cm^{-2} when deposited on a rotating disk electrode (RDE). Note, that when the catalysts are deposited on an MEA and their stability measured in a PEM electrolyser test unit, the duration they remain stable for during chronopotentiometric experiments will be increased (*ca.* 60,000 h).[57, 59, 60] However, the purpose of this study is to provide insight into how laboratory scale electrochemical techniques can be translated to commercial PEM electrolyser applications in the absence of such PEM electrolyser test units. Finally, there will be an overview of promising non-carbon supports for the anchoring of catalytic materials, which make up the anodic catalyst layer within a PEM cell. ESI Table 2 is an overview of recently studied optimal catalysts towards the OER in acidic media, where Figure 4 is a corresponding plot exhibiting the OER onset potential (V *vs.* RHE) against the over potential required to reach + 10 mA cm^{-2}. The OER onset is determined as the potential at which the Faradaic current commences, which is signified by the observed current deviating from the background current by the value of + 25 μA cm^{-2}.[63]

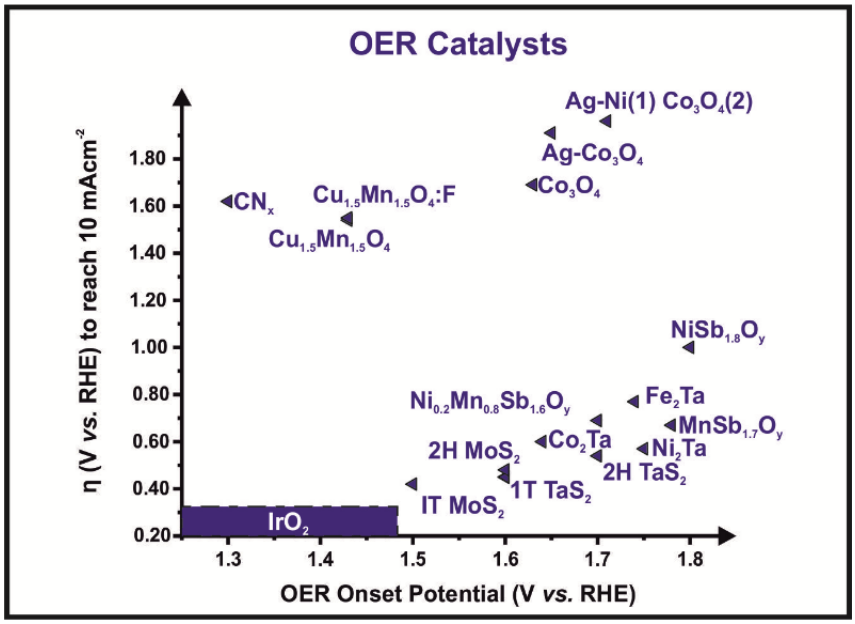

Figure 4 Graphical overview of optimal performing catalysts towards the oxygen evolution reaction (OER) within acidic media; OER onset potential (V *vs.* RHE) against the over potential or η (V) required to reach + 10 mA cm^{-2}. Optimal OER activity region occupied by IrO_2 shown for comparison.

3.1 Unary metal oxides

Unary metal oxides such as MnO_x, FeO_x, CoO_x and NiO_x have received considerable attention due to them being materials that show corrosion-resistant properties and good OER activity in acidic conditions. The stability of these oxides increases across the first row of transition metals (Ni to Mn), due an increase in the metal-oxygen bond strength, defining MnO_x as a highly stable material within low pH electrolytes.[134] However, the stability observed for MnO_x comes at the cost of reduced OER activity, being that four adjacent Mn^{III} sites are required to produce two Mn^{IV} sites (the phase required for oxygen bonding).[135] The small probability of coordinating four grouped Mn^{III} sites results in a material that exhibits poor OER activity in acidic media. Conversely, OER activity increases moving across the first row of the transition metals (Mn to Ni), owing to a weakening of the metal-oxygen interactions, which also results in reduced corrosion resistance. This activity trend is best described by the Sabatier principle, where the surface metal cations (M)

are the active sites for the OER. The principle states that catalysts with optimal M-O bond strength exhibit the best OER catalysis, whereas 'too strong' or 'too weak' M-O interactions lead to reduced OER activity. The OER proceeds with the following M-O bond intermediates: M-OH, M-O, M-OOH and M-OO.[136] McCrory *et al.*[126] benchmarked the performance of mixed metal oxides and unary metal oxides in 1 M H_2SO_4 based on OER activity, stability, ECSA and Faradaic efficiency. IrO_x, NiO_x, CoO_x, CoO_x^*, $NiCuO_x$, $NiCoO_x$, $NiFeO_x$ and $CoFeO_x$ were electrodeposited in varying mass incorporations separately upon glassy carbon (GC) electrodes and then explored towards the OER. All materials exhibited similar catalytic activity in acidic media, where the lowest over-potentials to reach + 10 mA cm^{-2} were exhibited by CoO_x* and $CoFeO_x$ (η= ~700 mV (*vs*. SCE)). The mass activities of the unary metal oxides are not reported within this study. However, literature mass activity values of 0.11, 0.04, 0.03 and 0.12 A g^{-1} correspond to CoO_x, NiO_x, FeO_x and $CoFeO_x$, respectively.[137] These values coincide with the findings by McCrory and co-workers given that CoO_x and $CoFeO_x$ exhibit mass activities closest to that of IrO_2 (*ca.* 0.30 A g^{-1}). The mass activity values exhibited by the metal oxides are not competitive with IrO_2, however financial incentives to implement these catalysts within the anode of PEM electrolysers could arise from the low cost of raw Co, Fe and Ni metal (< £0.05 g^{-1})[138] compared to the high cost of pure Ir metal (*ca.* £58.00 g^{-1}).[37] Only IrO_x exhibited stability in acidic conditions. The instability of each electrodeposited non-noble catalyst was outlined by cycling for 2 hours under oxidative conditions, given that all materials exhibited similar catalytic performance to the GC support. The observed instability arises when basic metal oxides come into contact with strong acids, protonation occurs throughout the metal oxide framework, resulting in weak M-O interactions.[139] The strongly acidic 1 M H_2SO_4 electrolyte is rarely used in catalysis studies and is likely not representative of the pH conditions within a PEM electrolyser. However, various studies have highlighted the instability of unary metal oxides in higher pH ranges of 2-3, in which certain mixed metal oxides exhibit stability.[134, 135, 140, 141]

Huynh *et al.*[142] designed a number of electrochemically active and acid-stable earth catalysts supported on FTO. Figure 5(A) depicts how Huynh and coworkers used the chemistry of unary metal oxides to synthesize composites that used MnO_x and PbO_x as stabilising elemental influences on highly active Co centres. Tafel analysis in 100 mM Phosphate & 1 M KNO_3 (pH 2.5) for the unary metal oxides CoO_x, FeO_x, MnO_x, PbO_x and IrO_x yielded values of 82, 51, 650, 121 and 32 mV dec^{-1}, respectively. It is important to observe the stabilizing effects of unary metal oxides

within mixed metal oxide films as a control. Mixed $CoMnO_x$ films electrodeposited at three different potentials (shown in Figure 5(B)) exhibit Tafel values similar to that of CoO_x at ~83 mV dec^{-1}, displaying no variation in OER activity. Pb was substituted for Mn as the structural element within the mixed metal oxides, where a Tafel value of ~72 mV dec^{-1} was observed for $CoPbO_x$. The presence of Mn and Pb in the composites provides a structural framework that prevents the reduction of the catalytic active sites through the elimination of O_2, which would lead to M-O bond weakening. Instead, the elements that provide structural frameworks are oxidised to more stable forms *i.e.* $PbO_x \rightarrow PbO_2$, hence providing a more corrosion resistant composite.[141] Chronopotentiometry was used to evaluate the long-term acid stability of the materials. For the OER at 0.1 mA cm^{-2} (shown in Figure 5(C)), $CoMnO_x$ electrodeposited at + 0.90 V exhibited an OER potential of + 1.5 V (*vs.* NHE) remaining undissolved after 12 hours, compared to + 2.0 V (*vs.* NHE) for MnO_x, remaining stable after 12 hours. Chronopotentiometry at + 1.0 mA cm^{-2} was used to further assess the stability of the mixed metal oxides (shown in Figure 5(C)), where $CoMnO_x$ electrodeposited at + 0.90 V dissolved after 30 mins. However, PbO_x demonstrated long term acidic stability at + 2.9 V (*vs.* NHE) for over 12h. The stabilizing role of unary metal oxides such as PbO_x and MnO_x within mixed metal oxides is evident and present a promising method for enhancing the stability of active transition metals.

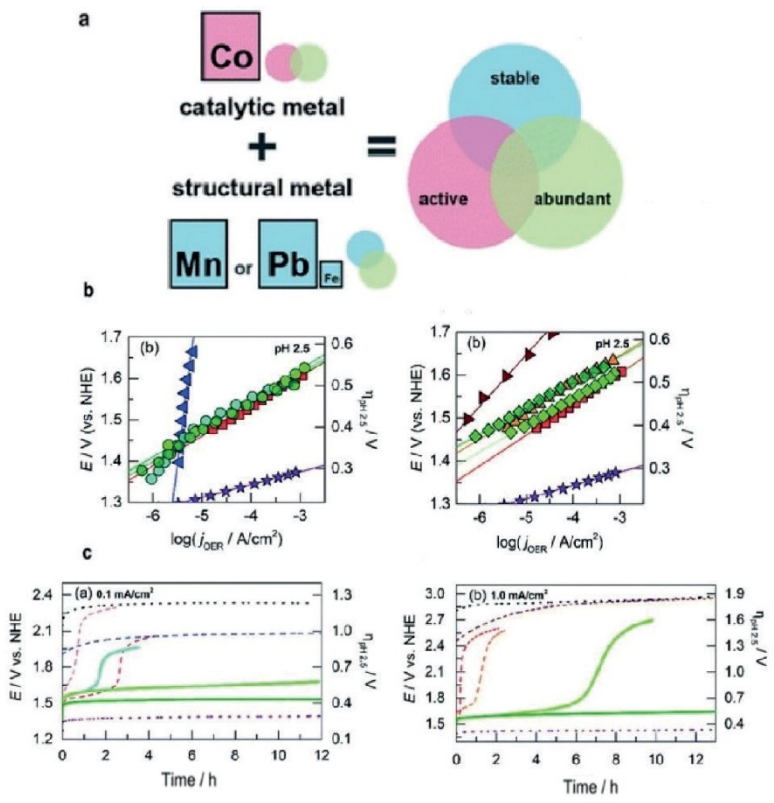

Figure 5 (A) Content overview outlining how properties such as activity and stability of the abundant non-precious metals Co, Mn, Pb and Fe can be combined to result in a proficient OER catalyst **(B)** Electrochemical stability for acidic OER measured by sustained chronopotentiometry at: 0.1 mA cm^{-2} in pH 2.5 P_i for $CoMnO_x$ deposited at 0.65 (light green ▬), 0.90 (dark green ▬), and 1.15 V (cyan ▬) with CoO_x (red ▬), NiO_x (light magenta ▬), MnO_x (blue ▬), IrO_x (purple ●●●), and FTO (grey ●●●). Then, 1.0 mA cm^{-2} in pH 2.5 P_i for $CoPbO_x$ (light green ▬) and $CoFePbO_x$ (dark green ▬) with $CoFeO_x$ (orange ▬), CoO_x (red ▬), and PbO_x (brown ▬) **(C)** Tafel plots for $CoMnO_x$ in 0.10 M P_i and 1.0 M KNO_3 at pH 2.5: $CoMnO_x$ deposited at 0.90 (dark green ●), 0.65 (light green ●), and 1.15 V (cyan ●), CoO_x (red ■), MnO_x (blue ◀), and IrO_x (purple ★). Then, pH 2.5 for $CoPbO_x$ (light green ♦) and $CoFePbO_x$ (dark green ♦), $CoFeO_x$ (orange ▲) and PbO_x (brown ▶) Adapted with permission from ref.[141]

3.2 Mixed metal oxides

It is clear that structural unary metal oxides enhance the stability of Co containing mixed metal oxide films. Huynh *et al*[141] demonstrated that the addition of structural oxides PbO_x and MnO_x

into active Co centres did not result in reduced OER catalysis. Huynh and co-workers deposited Pb ions in unison with $CoFeO_x$ films to result in a $CoFePbO_x$ composite that exhibited the optimal Tafel value of ~70 mV dec^{-1} (shown in Figure 5(B)). Chronopotentiometry at + 1.0 mA cm^{-2} was used to assess the stability of the $CoFePbO_x$ mixed film (shown in Figure 5(C)), which remained uncorroded at *ca.* + 1.8 V (*vs.* NHE) for over 50h of constant cycling. Mixed metal oxides are typically uncommon compositions of metal oxide based constituents, where the majority of studies do not state values of mass activity. However, it is expected that the mass activity of a mixed metal oxide will decrease with the addition of less active structural oxides such as PbO_x and MnO_x.

Mn and Pb are often utilised as structural frameworks to improve corrosion resistance within active metal oxides, however, unary MnO_x's are limited by poor OER catalysis. Adjustment of the transition metal *d*-band position relative to the fermi level is thought to increase the number of optimal interactions of reactant and product species at the catalytic active sites. An increase in the number of optimal reactant-product interactions facilitates efficient adsorption and desorption processes. As a result the OER onset potential is lowered.[143] Patel *et al.*[144] tuned the *d*-band in amorphous MnO_2 with Cu and F to match the fermi level of IrO_2 (− 1.33 eV). $Cu_{1.5}Mn_{1.5}O_4$ and $Cu_{1.5}Mn_{1.5}O_4$:F were synthesized by a facile procedure and supported on porous Ti foil, where F was incorporated in %wt variations to achieve the correct linear shift of the *d*-band towards that of IrO_2. The $Cu_{1.5}Mn_{1.5}O_4$ and $Cu_{1.5}Mn_{1.5}O_4$:F composites both exhibited OER onset potentials of + 1.43 V (*vs.* RHE), which matches the catalysis of IrO_2. The optimum incorporation of 10 %wt F into the $Cu_{1.5}Mn_{1.5}O_4$ composite, showed improvements in the current density at + 1.55 V (*vs.* RHE) where current densities of + 9.15, + 6.36 and + 7.74 mA cm^{-2} were displayed by the F-doped and non-doped composites, as well as IrO_2, respectively. The following results suggest that F doping enhances electrical conductivity of the composite at 10 wt% incorporation. Surrounding literature also suggests that F doping has a positive influence on the stability of transition metal catalysts within acidic conditions. This is due to an increase in the number of polar metal-F interactions with high binding energies.[145-149] Patel and co-workers carried out electrochemical stability studies that showed minimal deviation in OER performance over the course of 6000 cycles, with chronoamperometric measurements at + 1.55 V (vs. RHE), over a 24 hour duration also exhibiting no deviation in current density. However, there is a lack of long-term stability data to assess the suitability of fluorine doped metal oxides for anodic application within PEM electrolysers, where chronopotentiometric measurements for up to 200 hours and CV cycling for

a minimum of 50,000 cycles should be exhibited to compare against the benchmark IrO_2 catalyst. It is possible to impart greater stability and activity to mixed metal oxides with the addition of Sb, which is thermally stable.[150] Moreno-Hernandez *et al.*[151] sputter coated $Ni_xMn_{1-x}Sb_{1.6-1.8}O_y$ species based catalysts onto conductive films of antimony-doped tin oxide (ATO) and evaluated catalytic activity in 1.0 M H_2SO_4 by cyclic voltammetry and chronopotentiometry. In general, films containing both Ni and Mn exhibited the lowest overpotentials, where the lowest over potential of 672 mV (*vs.* RHE) was displayed by $Ni_{0.5}Mn_{0.5}Sb_{1.7}O_y$. Chronopotentiometry under galvanostatic control at 10 mA cm^{-2} and cyclic voltammetry outlined that $Ni_xMn_{1-x}Sb_{1.6-1.8}O_y$ was stable for more than 150 hours, with negligible increases in over potential. At several points during chronopotentiometric measurements, ICP-MS was used to determine the concentration of dissolved solids within the acidic electrolyte, where 56, 17 and 11% of the Mn, Ni and Sb, respectively, had leached from the $Ni_{0.5}Mn_{0.5}Sb_{1.7}O_y$ electrode after 144 hours. The leaching of Mn within the composite provides a stable structural framework around the active surface of Ni leading to enhanced OER catalysis.[152] Further stability of the composite is explained by the formation of the crystalline MSb_2O_6 rutile-type phase. The remarkable observations within this study outline the most stable phase of mixed metal oxides through the doping of the composite with antimony. Incorporation of $Ni_{0.5}Mn_{0.5}Sb_{1.7}O_y$ into the catalyst layer of the anodic side of a PEM electrolyser would exhibit a 57% Faradaic efficiency.[151]

3.3 Beyond metal oxides

TMD's typically exhibit good OER activity,[153, 154] however suffer from dissolution in acidic conditions and poor stability in a highly oxidative environment, which hampers their application within PEM electrolysers.[83] Wu *et al.*[155] exfoliated MoS_2 and TaS_2 nanosheets using liquid phase and lithium intercalation and assessed the catalysis of the trigonal prismatic (2H) versus the octahedral (1T) phases in 0.5 M H_2SO_4. The overpotentials to reach + 10 mA cm^{-2} of 420, 450, 480 and 540 mV (*vs.* RHE) for 1T-MoS_2, 1T-TaS_2, 2H-MoS_2 and 2H-TaS_2 are comparable to that of IrO_2 (390 mV *vs.* RHE). Density functional theory (DFT) calculations outline that the catalysis exhibited by the TMD's is a result of the HET at the edge sites. Energy profiles of the IT and 2H phases of MoS_2 and TaS_2 show that the lowest activation barriers are exhibited by the 1T phase. The stability of each material in acidic media is poor. Chronopotentiometric curves using 1T-MoS_2 were recorded at + 10 mA cm^{-2} after 2000 cycles between + 1.2 and + 2.0 V (*vs.* RHE). There was

a marked increase in onset potential from + 1.6-1.7 V (*vs.* RHE) after 2h, suggesting poor stability in acidic and oxidative conditions.

Intermetallic alloys can consist of highly active transition metals, that are typically prone to dissolution in acidic media (Ni, Co and Fe), with corrosion resistant early transition metals (V, Nb and Ta). This combination can create stable catalysts that are potentially suitable as the anodic catalyst layers within PEM electrolysers. Mondschein *et al.*[156] synthesized first row transition metal alloys with Ta *via* high temperature and metallurgical routes. These alloys exhibit stable properties in acidic media relative to the single element components Ni, Fe and Co. The crystal structure of the intermetallic alloys is shown in Figure 6(A) using Ni_2Ta as an example, which is the most catalytically active and stable anode material in acidic conditions. Ni_2Ta rods were arc melted and their OER activity was assessed in 0.5 M H_2SO_4 with polycrystalline powders of Ni_2Ta, Co_2Ta and Fe_2Ta. Overpotentials of 980, 570, 600 and 770 mV (*vs.* RHE) were observed at + 10 mA cm^{-2}, respectively (shown in Figure 6(B)). The Ni_2Ta rods exhibited no deviation in OER performance during galvanostatic measurements at 10 mA cm^{-2} for 3 days. Corrosion resistance of the Ni_2Ta rods was assessed by ICP-OES, which was used to measure time dependent dissolution of Ni and Ta from the Ni_2Ta rods, shown in Figures 5(C and D). A pure Ni control rod leached 43.6 μg min^{-1} of Ni, whereas the Ni_2Ta rods exhibited Ni dissolution of only 0.393 μg min-^{1}. This is superior to the corrosion data obtained for IrO_2 and RuO_2 within 0.5 M H_2SO_4. The rate of Ta dissolution was 0.15 ng min^{-1}, hence highlighting the formation of TaO_x upon dissolution of Ni, where TaO_x is known to be highly stable in acidic media. Like Mn and Pb, Ta has the potential to be incorporated into the structures of active OER materials to enhance stability and corrosion resistance. This should be considered in future studies. Note that Wu, Mondschein and co-workers did not state values of mass activity for their catalysts and representative comparisons may not be stated.

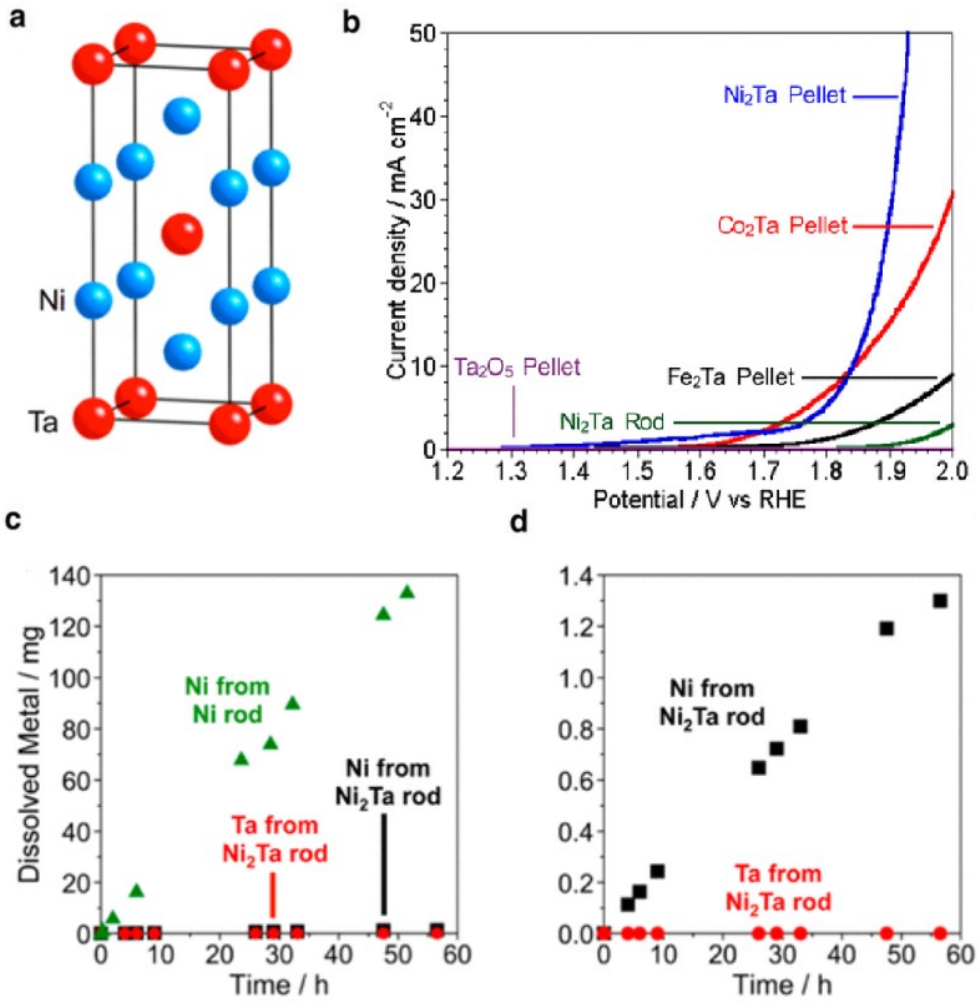

Figure 6 (A) Crystal structure of Ni_2Ta showing the positions of the Ni (blue) and Ta (red) atoms. **(B)** Linear sweep voltammograms of a Ni_2Ta rod and polycrystalline powders consisting of Ni_2Ta, Fe_2Ta, and Co_2Ta. **(C)** ICP-OES data characterizing the time-dependent dissolution of Ni and Ta from a Ni rod and Ni_2Ta rod. **(D)** Time-dependent dissolution data for the Ni_2Ta rod, magnified from the plot in panel (C). Adapted with permission from ref.[156]

3.4 Stable anodic conductive supports

The suitability of a catalyst material for use within PEM electrolysis is not only based on the active material. Promising catalysts are anchored upon supporting materials for a number of reasons: reducing the cost of the catalyst-coated membrane (CCM) by reducing catalyst loading; enhancing electrical conductivity of the catalyst layer; increasing lifetime of the CCM; and providing a large surface area for catalyst deposition.[157-159]

Excellent electrical conductivity and high surface area for catalyst dispersion are properties that shape carbon-based materials as effective catalyst supports within fuel cells and the cathodic side of PEM electrolysers. Anchoring cathodic catalyst materials to carbon-based supports has many benefits: carbon supports provide electronic conduction pathways between the electrode and the catalyst; carbon supports allow catalytic materials to be deposited on a nanoparticle level; and carbon materials are also durable in acidic media.[160] Catalyst supports are therefore key to the current output of the electrolyser and its longevity.[161-165] However, carbon based supports are not suitable for application within the anodic side of electrolysers given that they suffer fast corrosion under high oxidative potentials.[166]

Effective support materials can enhance the electro kinetics of the anodic catalyst layer. Increasing the electroactive surface area allows for the optimal surface dispersion of highly active particles that lower the OER onset potential. This increase in surface area also enables the low loading of active catalyst materials thus reducing the costing associated with the MEA. Degradation of the catalyst layers can result in reduced system and stack lifetimes within PEM electrolyser cells.[167] Therefore, research of corrosion resistant materials provides a pathway to increasing the lifetime of PEM electrolyser technologies. Titanium is typically used as the anodic support material within PEM electrolysers.[168] Titanium (TiO_2) and tin oxides (SnO_2) have been studied as alternative OER supports given their high resistance to anodic oxidative conditions, however are mainly utilised as supports for IrO_2 or RuO_2 within the literature and are limited by their poor electronic conductivity ($\sim 10^{-6}$ S cm^{-1}).[169-174]

One study utilising a TiO_2 support for a noble metal free OER catalyst is by Zhao *et al.*[175] who embedded iron oxide within titania nanowires (Fe_2O_3/TiO_2 NWs). The Fe_2O_3/TiO_2 NWs and Fe_2O_3 supported on Ti foam exhibited OER onset potentials of + 1.46 and + 1.63 V (*vs.* RHE). Given that Fe_2O_3 is unstable in acidic media within anodic oxidative conditions, it is important to assess

the stabilizing effect of the titania nanowires. Chronopotentiometry at + 1.9 V (*vs.* SCE) for 20 h in 0.5 M H_2SO_4 displayed current density decays of 30.3 and 66.7% for the Fe_2O_3/TiO_2 NWs and Fe_2O_3 supported on Ti foam, respectively. It is clear that Fe_2O_3 embedded within titania nanowires experiences less current degradation than its counterpart without a titania support. Antimony doped tin oxide (ATO) is a support material highlighted for its high conductivity (0.57 S cm^{-1}), thermal stability (> 250 °C) and acid stability in oxidative conditions.[176, 177] Jaouen *et al*[178] supported Cobalt hexacyanoferrate nanoparticles upon ATO (ATO@CoHFe), where the ATO@17% CoHFe (*39.7 mg ATO and 8 mg CoHFe*) exhibited optimal OER catalysis with an onset potential of 1.80 V (*vs.* RHE), compared to the negligible OER catalysis exhibited by the unmodified ATO support. The stability of the ATO@17% CoHFe was probed within a PEM electrolyser cell at a fixed voltage of + 2.0 V for 22 h, where a 10 % degradation in current density was observed. The cell potential was ramped to + 2.2 V, where a significant degradation in current density was observed, which was attributed to leaching within the ATO support. Quantification of the dissolved ATO support was carried out by ICP-MS, where at a cell voltage of + 2.0 V elemental losses for Sn and Sb were 0.16 and 8.5 %, respectively. When the potential was ramped to + 2.2 V, elemental losses of 22.6 and 52.7% were recorded for Sn and Sb, respectively. These findings are unprecedented given that ATO has only been reported to be stable at cell voltages up to + 1.8 V.[179-181] The above studies challenge the application of titania or ATO as anodic catalyst support systems within PEM electrolyser cells, particularly at high oxidative potentials (> + 1.8 V) where significant current degradation and elemental dissolution is observed. It is evident that more research needs to be carried out regarding non precious metals supported on highly stable conductive substrates. The studies within this area are sparse and typically focus on precious metal catalysts such as IrO_2 or RuO_2.

4 Summary

In order to summarize the research reviewed herein, an emphasis will be placed on the stability of the HER and OER catalysts as this is typically the principal factor in determining whether a catalyst is suitable for operation within a PEM electrolyser. Plenty of HER studies report on catalysts that exhibit excellent HER catalysis and compare that to the near zero overpotential of the benchmark Pt/C catalyst; as a result there is a plethora of proficient HER catalysts within literature. However, the vast majority of these studies evaluating HER specific catalysts contain limited information on the long-term durability of their catalysts, thus a definitive conclusion on their suitability within PEM electrolysis is challenging. It would be natural to assume that if the HER activity of each catalyst were benchmarked against Pt/C, then their stability should also be benchmarked against Pt/C. This is a critical measurement given that the partial degradation of a PEM electrolysers performance may be attributed to the Pt based cathode.[62] However, of all the HER studies reviewed herein, only two catalysts are tested using chronopotentiometry for a duration longer than 20 hours, as shown in ESI table 1, where Pt/C is known to remain stable for more than 50 hours.[58] None of these HER studies coincide their stability measurements with ICP-MS measurements, thus there is a lack of information pertaining to leaching within HER specific catalysts. There is progress within the synthesis of HER catalysts, where alloying active metals such as Ni, Fe or Co with highly stable metals such as Pb, Zn, Sb, Ta or Mn creates a structural framework that exhibits promising stability in acidic conditions. This is also observed when active metal centres are doped with optimal quantities of phosphorus, such as CP@Ni-P which remains stable after 150 hours of chronopotentiometry at − 10 mA cm^{-2} in acidic conditions.[122]

It is often the case that more comprehensive stability examinations take place in studies regarding OER specific catalysts. This is likely due to the high oxidative potentials at the surface of the anode as the Faradaic process of the OER proceeds. Because of this, many studies deposit OER specific catalysts on non-carbon based supports such as ATO or FTO. Studies that support their OER specific catalysts on carbonaceous materials are uninstructive on the basis that data obtained by this method is not translational to commercial PEM electrolysis. However, the majority of studies that take this factor into account carry out more extensive stability studies, involving chronopotentiometric measurements for 50 hours or more, coupled with ICP-MS analysis. The same principles for catalyst synthesis used in HER catalysis apply to OER catalysts too, where stable elements provide a structural framework for active metals and therefore high stability. OER

catalysts such as: Ni_2Ta,[156] $MnSb_{1.7}O_y$, $NiSb_{1.8}O_y$ and $Ni_{0.5}Mn_{0.5}Sb_{1.7}O_y$[151] synthesised using these principals achieve catalyst durability from 70-200 hours, where the benchmark OER catalyst IrO_2, is known to remain stable for up to 200 hours during chronopotentiometric measurements.[57]

Another key consideration for the application of NPM catalysts at the anode or cathode of a PEM electrolyser is mass activity (current output per unit mass). This activity metric merges catalyst loading and current output to differentiate between excellent catalysis because of ultra-high catalyst loading, and relative catalysis with low catalyst loading.[182] If the mass activities of NPM HER and OER catalysts are benchmarked against the mass activities of the precious metal catalysts currently utilized in commercial PEM electrolysis, the economic viability of these catalysts for use within PEM electrolysers can be calculated based on required quantities and cost of raw materials. However, mass activity is not reported in the majority of studies utilising NPM HER and OER catalysts, but is regularly provided in studies regarding precious metal based catalysts.[55, 133, 183] It is common within the literature for mass activities to be reported at a range of different potential values, making comparisons between the mass activities of different catalysts impractical.[55, 184] Therefore it is suggested that future studies calculate mass activity at a standard overpotential value of 200 mV (*vs.* RHE).[104, 185, 186]

6 *Conclusions and future perspectives*

We have provided a thorough overview of the literature reporting non-precious metal materials utilised to catalyse the HER and OER. In order for any of the catalysts described herein to be applicable for use within a PEM electrolyser they must show comparable achievable current densities and onset potentials to their precious metal counterparts as well as display excellent stability and minimal leaching in acidic conditions. Whilst some of the reviewed catalysts displayed promising properties, many displayed inapplicable catalyst stability testing for commercial electrolyser applications. Therefore, we propose that the following four stability-testing procedures are implemented, for HER and OER catalysts, within future studies to make their results applicable to real-world electrolysers and universally comparable:

- Chronopotentiometric measurements at varied current densities: 10, 20 and 50 mA cm^{-2}, for *at least* 200 hours, to assess the ability of the catalyst to maintain a stable current at a set potential over a long duration. This significantly lengthens the duration of chronopotentiometric measurements currently used in literature.[187-189]
- ICP-MS measurements are critical analyses of catalyst activity and durability however are sparsely used in literature.[190-192] Therefore, we propose that all studies should include ICP-MS measurements carried out in unison with chronopotentiometric measurements to assess the rate of leaching of the active component within a catalyst in acidic media.
- Cyclic voltammetry (CV) is typically carried out for a maximum of 10,000 cycles.[118-120] We propose, cyclic voltammetry for a minimum of 50,000 cycles, within a potential range (V *vs*. RHE) where the HER or OER onset potential and a current density of + or − 10 mA cm^{-2} can be observed. This will assess whether the onset potential has diminished over the course of repeat Faradaic processes.
- Where possible, X-ray photoelectron spectroscopy (XPS) of the catalyst surface should be used to quantify any changes to elemental composition before and after long-term stability measurements. This technique may also be used to identify catalyst phases responsible for specific electrochemical properties, hence provides crucial information on how to tune catalysts to exhibit optimal activity and stability.[193-195]
- Mass activity (A g^{-1}) at an overpotential of 200 mV (*vs.* RHE) is a key activity metric to assess the feasibility of a NPM catalysts implementation within a PEM electrolyser

and should be benchmarked against mass activities exhibited by the currently utilized commercial precious metal catalysts.[57, 196]

This stability-testing regime more accurately mimics the conditions within an operating electrolyser with fivefold increases in the duration of chronopotentiometric measurements and the number of CV cycles compared to stability testing regimes in alternative studies. Future work regarding NPM HER and OER catalysts should focus on alloying active metals such as Ni, Fe and Co with transition metals that promote structural stability Mn, Pb, Zn, Ta or Sb. These structural frameworks have been shown to exhibit promising activity and stability in acidic conditions. Similar results are observed within HER specific materials when doping active metal centres with optimal quantities of phosphorus. The use of these principals to synthesise stable NPM catalysts coupled with the proposed testing regime will inform future research into catalysts that have the potential to be used for water splitting within PEM electrolysers.

Acknowledgements

This study is funded by Innovate UK (Reference: 11607) in cooperation with the European Marine Energy Centre (EMEC). Funding is also from the Engineering and Physical Sciences Research Council (Reference: EP/P007767/1 and EP/N0011877/1). The Manchester Fuel Cell Innovation Centre is funded by the European Regional Development Fund. Permission has been granted for all figures and graphics used within this review article.

Conflicts of Interest

There are no conflicts of interest to declare.

References

[1] G. Thomas, Overview of Storage Development DOE Hydrogen Program, Hydrogen Program Review, Livermore, CA, 2000.
[2] D. Rand, A journey on the electrochemical road to sustainability, J. Solid State Electrochem. **15**(7) (2011) 1579-1622.
[3] O.O.E.E.R. Energy, Hydrogen Production Processes, in: U.S.D.o. Energy (Ed.) 2019.
[4] N.Kornienko, N.Heidary, G.Cibin, E.Reisner, Catalysis by design: development of a bifunctional water splitting catalyst through an operando measurement directed optimization cycle, Chem. Sci. **9**(24) (2018) 5322-5333.
[5] J. Song, C. Zhu, B. Xu, S. Fu, M.H. Engelhard, R. Ye, D. Du, S.P. Beckman, Y. Lin, Bimetallic Cobalt-Based Phosphide Zeolitic Imidazolate Framework: CoPx Phase-Dependent Electrical Conductivity and Hydrogen Atom Adsorption Energy for Efficient Overall Water Splitting, Adv. Energy Mater. **7**(2) (2017) 1601555.
[6] Q. Lu, G.S. Hutchings, W. Yu, Y. Zhou, R.V. Forest, R. Tao, J. Rosen, B.T. Yonemoto, Z. Cao, H. Zheng, J. Xiao, F. Jiao, J.Y.C. Chen, Highly porous non-precious bimetallic electrocatalysts for efficient hydrogen evolution, Nat. Commun. **6**(1) (2015) 6567.
[7] S.I. Maintinguer, R.R. Hatanaka, J.E. de Oliveira, Glycerol as a Raw Material for Hydrogen Production, Biofuels - Status and Perspective2015.
[8] H. Pan, Tension-Enhanced Hydrogen Evolution Reaction on Vanadium Disulfide Monolayer, Nanoscale Res. Lett. **11**(1) (2016) 113-113.
[9] A. Keçebaş, M. Kayfeci, M. Bayat, Chapter 9 - Electrochemical hydrogen generation, in: F. Calise, M.D. D'Accadia, M. Santarelli, A. Lanzini, D. Ferrero (Eds.), Solar Hydrogen Production, Academic Press2019, pp. 299-317.
[10] K. Zeng, D. Zhang, Recent progress in alkaline water electrolysis for hydrogen production and applications, Prog. Energy Combust. Sci. 36(3) (2010) 307-326.
[11] V. Nikolic, G. Tasic, A. Maksic, D.P. Saponjic, S.M. Miulovic, M.P. Marceta Kaninski, Raising efficiency of hydrogen generation from alkaline water electrolysis – Energy saving, Int. J. Hydrogen Energy 35(22) (2010) 12369-12373.
[12] M.A. Laguna-Bercero, Recent advances in high temperature electrolysis using solid oxide fuel cells: A review, J. Power Sources 203 (2012) 4-16.
[13] R. Knibbe, M. Traulsen, A. Hauch, S. Ebbesen, M. Mogensen, Solid Oxide Electrolysis Cells: Degradation at High Current Densities, J. Electrochem. Soc. 157 (2010) B1209-B1217.
[14] M. Carmo, D.L. Fritz, J. Mergel, D. Stolten, A comprehensive review on PEM water electrolysis, Int. J. Hydrogen Energy 38(12) (2013) 4901-4934.
[15] M. Reisert, A. Aphale, P. Singh, Solid Oxide Electrochemical Systems: Material Degradation Processes and Novel Mitigation Approaches, Materials 11(11) (2018) 2169.
[16] M.S. Sohal, J.E. O'Brien, C.M. Stoots, V.I. Sharma, B. Yildiz, A. Virkar, Degradation Issues in Solid Oxide Cells During High Temperature Electrolysis, ASME 2010 8th International Conference on Fuel Cell Science, Engineering and Technology, 2010, pp. 377-387.
[17] D. Symes, B. Duri, A. Dhir, W. Bujalski, B. Green, A. Shields, M. Lees, Design for On-Site Hydrogen Production for Hydrogen Fuel Cell Vehicle Refueling Station at University of Birmingham, U.K, Energy Procedia **29** (2012) 606–615.
[18] P. Nikolaidis, A. Poullikkas, A comparative overview of hydrogen production processes, Renewable Sustainable Energy Rev. **67** (2017) 597-611.
[19] P. Millet, R. Ngameni, S. Grigoriev, N. Mbemba, F. Brisset, A. Ranjbari, C. Etiévant, PEM water electrolyzers: From electrocatalysis to stack development, Int. J. Hydrogen Energy **35**(10) (2010) 5043-5052.
[20] F.J. Wirkert, J. Roth, S. Jagalski, P. Neuhaus, U. Rost, M. Brodmann, A modular design approach for PEM electrolyser systems with homogeneous operation conditions and highly efficient heat management, Int. J. Hydrogen Energy (2019).
[21] M. Santarelli, P. Medina, M. Calì, Fitting regression model and experimental validation for a high-pressure PEM electrolyzer, Int. J. Hydrogen Energy 34(6) (2009) 2519-2530.
[22] R. Clarke, S. Giddey, F. Ciacchi, S. Badwal, B. Paul, J. Andrews, Direct coupling of an electrolyser to a solar PV system for generating hydrogen, Int. J. Hydrogen Energy **34**(6) (2009) 2531-2542.

[23] O.E. Herrera, D.P. Wilkinson, W. Mérida, Anode and cathode overpotentials and temperature profiles in a PEMFC, J. Power Sources 198 (2012) 132-142.
[24] M.A.Z.G. Sial, S. Baskaran, A. Jalil, S.H. Talib, B. Lin, Y. Yao, Q. Zhang, H. Qian, J. Zou, X. Zeng, NiCoFe oxide amorphous nanohetrostructres for oxygen evolution reaction, Int. J. Hydrogen Energy **44**(41) (2019) 22991-23001.
[25] Z. Lv, Y. Zhang, K. Wang, T. Yu, X. Liu, G.G. Wang, G. Xie, L. Jiang, High performance of Co–P/NF electrocatalyst for oxygen evolution reaction, Mater. Chem. Phys. **235** (2019) 121772.
[26] N.-T. Suen, S.-F. Hung, Q. Quan, N. Zhang, Y. Xu, H. Chen, Electrocatalysis for the oxygen evolution reaction: recent development and future perspectives, Chem. Soc. Rev. **46**(2) (2017) 337-365.
[27] X. Wen, J. Guan, Recent progress on MOF-derived electrocatalysts for hydrogen evolution reaction, Appl. Materials Today **16** (2019) 146-168.
[28] S. Shiva Kumar, V. Himabindu, Hydrogen production by PEM water electrolysis – A review, Materials Science for Energy Technologies 2(3) (2019) 442-454.
[29] J.-Q. Chi, H. Yu, Water electrolysis based on renewable energy for hydrogen production, Chin. J. Catal. **39**(3) (2018) 390-394.
[30] P.E.L.o.b.o. Cadent, HyMotion - Network-supplied hydrogen unlocks low carbon transport opportunities, 2019, p. 6.
[31] F. Birol, How hydrogen can offer a clean energy future, Financial Times, 04/06/2019.
[32] S. Cherevko, T. Reier, A.R. Zeradjanin, Z. Pawolek, P. Strasser, K.J.J. Mayrhofer, Stability of nanostructured iridium oxide electrocatalysts during oxygen evolution reaction in acidic environment, Electrochem. Commun. 48 (2014) 81-85.
[33] J. Zhang, A.-J. Wang, Z. Liao, P. Zhang, F. Wang, X. Zhuang, E. Zschech, X. Feng, Iridium nanoparticles anchored on 3D graphite foam as a bifunctional electrocatalyst for excellent overall water splitting in acidic solution, Nano Energy 40 (2017) 27-33.
[34] S. Sun, G. Zhang, D. Geng, Y. Chen, R. Li, M. Cai, X. Sun, A Highly Durable Platinum Nanocatalyst for Proton Exchange Membrane Fuel Cells: Multiarmed Starlike Nanowire Single Crystal, Angew. Chem., Int. Ed. **50**(2) (2011) 422-426.
[35] S. Thoi, R.E. Usiskin, S.M. Haile, Platinum-decorated carbon nanotubes for hydrogen oxidation and proton reduction in solid acid electrochemical cells, Chem. Sci. **6**(2) (2015) 1570-1577.
[36] L.B.M.A. (LBMA), Precious metals prices 2019. http://www.lbma.org.uk/precious-metal-prices.
[37] J. Matthey, Precious metal prices, 2019. http://www.platinum.matthey.com/prices/price-charts#.
[38] U.M. Research, Iridium Catalyst Market Size, Share, Trends, Growth, Forecast Analysis Report By Product, By Application, By Segment, By Region - Global Forecast To 2025, 2019. https://www.upmarketresearch.com/reports/iridium-catalyst-market-research-report-2019.
[39] F. Du, Y. Zhang, H.Y. He, L. Li, G. Wen, Y. Zhou, Z. Zou, Electrodeposited amorphous cobalt phosphosulfide on Ni foams for highly efficient overall water splitting, J. Power Sources **431** (2019) 182-188.
[40] L. Zhang, Y. Li, J. Peng, K. Peng, Bifunctional NiCo2O4 porous nanotubes electrocatalyst for overall water-splitting, Electrochim. Acta **318** (2019) 762-769.
[41] J.P. Hughes, F.D. Blanco, C. Banks, S. Rowley-Neale, Mass-producible 2D-WS2 bulk modified screen printed electrodes towards the hydrogen evolution reaction, RSC Adv. **9**(43) (2019) 25003-25011.
[42] B.-W. Ahn, T.-Y. Kim, S.C. Kim, Y.-I. Song, S.-J. Suh, Amorphous MoS2 nanosheets grown on copper@nickel-phosphorous dendritic structures for hydrogen evolution reaction, Appl. Surf. Sci. **432** (2018) 183-189.
[43] B. Askari, P. Salarizadeh, M. Seifi, S.M. Rozati, A. Beheshti-Marnani, H. Saeidfirozeh, MoCoFeS hybridized with reduced graphene oxide as a new electrocatalyst for hydrogen evolution reaction, Chem. Phys. Lett. **711** (2018) 32-36.
[44] C. Tsai, K. Chan, F. Abild-Pedersen, J. Nørskov, Active edge sites in MoSe2 and WSe2 catalysts for the hydrogen evolution reaction: a density functional study, Phys. Chem. Chem. Phys 16(26) (2014) 13156-13164.
[45] Y. Liu, J. Liu, Z. Li, X. Fan, Y. Li, F. Zhang, G. Zhang, G. Peng, S. Wang, Exfoliated MoS2 with porous graphene nanosheets for enhanced electrochemical hydrogen evolution, Int. J. Hydrogen Energy **43**(30) (2018) 13946-13952.
[46] B. Han, Y. Hu, MoS2 as a co-catalyst for photocatalytic hydrogen production from water, Energy Sci. Eng. **4**(5) (2016) 285-304.
[47] C. Wang, Z. Yu, X. Wang, B. Lin, Enhanced electrocatalytic performance of NiOx@MnOx@graphene for oxygen reduction and evolution reactions, Int. J. Hydrogen Energy (2018).

[48] J. Benson, M. Li, S. Wang, P.-N. Wang, P. Papakonstantinou, Electrocatalytic Hydrogen Evolution Reaction on Edges of a Few Layer Molybdenum Disulfide Nanodots, ACS Appl. Mater. Interfaces **7**(25) (2015) 14113-14122.
[49] M. Imran, A.B. Yousaf, S.J. Zaidi, C. Fernandez, Tungsten-molybdenum oxide nanowires/reduced graphene oxide nanocomposite with enhanced and durable performance for electrocatalytic hydrogen evolution reaction, Int. J. Hydrogen Energy **42**(12) (2017) 8130-8138.
[50] M.Ahmed, B.Choi, Y.Kim, Development of Highly Active Bifunctional Electrocatalyst Using Co(3)O(4) on Carbon Nanotubes for Oxygen Reduction and Oxygen Evolution, Sci. Rep **8**(1) (2018) 2543-2543.
[51] H. Begum, J.-P. Jeon, Highly efficient and stable bifunctional electrocatalyst for water splitting on Fe–Co3O4/carbon nanotubes, Int. J. Hydrogen Energy **43**(11) (2018) 5522-5529.
[52] J. Wang, W. Chen, X. Wang, E. Wang, N-doped graphene supported WxC composite material as an efficient non-noble metal electrocatalyst for hydrogen evolution reaction, Electrochim. Acta 251 (2017) 660-671.
[53] S. Rowley-Neale, D.A.C. Brownson, G. Smith, D.A.G. Sawtell, P. Kelly, C. Banks, 2D nanosheet molybdenum disulphide (MoS2) modified electrodes explored towards the hydrogen evolution reaction, Nanoscale 7(43) (2015) 18152-18168.
[54] J. Kibsgaard, I. Chorkendorff, Considerations for the scaling-up of water splitting catalysts, Nature Energy 4(6) (2019) 430-433.
[55] N. Cheng, S. Stambula, D. Wang, M.N. Banis, J. Liu, A. Riese, B. Xiao, R. Li, T.-K. Sham, L.-M. Liu, G.A. Botton, X. Sun, Platinum single-atom and cluster catalysis of the hydrogen evolution reaction, Nature Communications 7(1) (2016) 13638.
[56] H. Yang, C. Wang, F. Hu, Y. Zhang, H. Lu, Q. Wang, Atomic-scale Pt clusters decorated on porous α-Ni(OH)2 nanowires as highly efficient electrocatalyst for hydrogen evolution reaction, Science China Materials 60 (2017) 1-8.
[57] M. Bernt, A. Hartig-Weiß, M.F. Tovini, H.A. El-Sayed, C. Schramm, J. Schröter, C. Gebauer, H.A. Gasteiger, Current Challenges in Catalyst Development for PEM Water Electrolyzers, Chem. Ing. Tech. 92(1-2) (2020) 31-39.
[58] K. Li, Y. Li, Y. Wang, J. Ge, C. Liu, W. Xing, Enhanced electrocatalytic performance for the hydrogen evolution reaction through surface enrichment of platinum nanoclusters alloying with ruthenium in situ embedded in carbon, Energy Environ. Sci. 11(5) (2018) 1232-1239.
[59] K. Bareiß, C. de la Rua, M. Möckl, T. Hamacher, Life cycle assessment of hydrogen from proton exchange membrane water electrolysis in future energy systems, Applied Energy 237 (2019) 862-872.
[60] E. Price, Durability and Degradation Issues in PEM Electrolysis Cells and its Components, Johnson Matthey Technology Review 61 (2017) 47-51.
[61] P. Shirvanian, F. van Berkel, Novel components in Proton Exchange Membrane (PEM) Water Electrolyzers (PEMWE): Status, challenges and future needs. A mini review, Electrochemistry Communications 114 (2020) 106704.
[62] E. Brightman, J. Dodwell, N. van Dijk, G. Hinds, In situ characterisation of PEM water electrolysers using a novel reference electrode, Electrochemistry Communications 52 (2015) 1-4.
[63] L. Cheng, W. Huang, Q. Gong, C. Liu, Z. Liu, Y. Li, H. Dai, Ultrathin WS2 Nanoflakes as a High-Performance Electrocatalyst for the Hydrogen Evolution Reaction, Angew. Chem. Int. Ed. 126(30) (2014) 7994-7997.
[64] D. Kong, H. Wang, J.J. Cha, M. Pasta, K.J. Koski, J. Yao, Y. Cui, Synthesis of MoS2 and MoSe2 Films with Vertically Aligned Layers, Nano Lett. **13**(3) (2013) 1341-1347.
[65] W. Guo, Y. Chen, L. Wang, J. Xu, D. Zeng, D.-L. Peng, Colloidal synthesis of MoSe2 nanonetworks and nanoflowers with efficient electrocatalytic hydrogen-evolution activity, Electrochim. Acta **231** (2017) 69-76.
[66] K. Hu, J. Zhou, Z. Yi, C. Ye, H. Dong, K. Yan, Facile synthesis of mesoporous WS2 for water oxidation, Appl. Surf. Sci. 465 (2019) 351-356.
[67] Z. Wu, B. Fang, A. Bonakdarpour, A. Sun, D.P. Wilkinson, D. Wang, WS2 nanosheets as a highly efficient electrocatalyst for hydrogen evolution reaction, Appl. Catal., B 125 (2012) 59-66.
[68] R.Chaurasiya, A.Dixit, R.Pandey, Strain-mediated stability and electronic properties of WS2, Janus WSSe and WSe2 monolayers, Superlattices Microstruct. 122 (2018) 268-279.
[69] X. Chia, A.Y.S. Eng, A. Ambrosi, S.M. Tan, M. Pumera, Electrochemistry of Nanostructured Layered Transition-Metal Dichalcogenides, Chem. Rev. **115**(21) (2015) 11941-11966.
[70] H. Wang, Z. Lu, D. Kong, J. Sun, T.M. Hymel, Y. Cui, Electrochemical Tuning of MoS2 Nanoparticles on Three-Dimensional Substrate for Efficient Hydrogen Evolution, ACS Nano **8**(5) (2014) 4940-4947.

[71] S.Watzele, J.Fichtner, B.Garlyyev, N.Schwämmlein, A.Bandarenka, On the Dominating Mechanism of the Hydrogen Evolution Reaction at Polycrystalline Pt Electrodes in Acidic Media, ACS Catalysis **8**(10) (2018) 9456-9462.
[72] X. Gan, L.Y.S. Lee, K.-y. Wong, T.W. Lo, K.H. Ho, D.Y. Lei, H. Zhao, 2H/1T Phase Transition of Multilayer MoS2 by Electrochemical Incorporation of S Vacancies, ACS Appl. Energy Mater. **1**(9) (2018) 4754-4765.
[73] D. Voiry, M. Salehi, R. Silva, T. Fujita, M. Chen, T. Asefa, V.B. Shenoy, G. Eda, M. Chhowalla, Conducting MoS2 Nanosheets as Catalysts for Hydrogen Evolution Reaction, Nano Letters 13(12) (2013) 6222-6227.
[74] D. Escalera-López, Y. Niu, S.J. Park, M. Isaacs, K. Wilson, R.E. Palmer, N.V. Rees, Hydrogen evolution enhancement of ultra-low loading, size-selected molybdenum sulfide nanoclusters by sulfur enrichment, Applied Catalysis B: Environmental 235 (2018) 84-91.
[75] M.Bernt, A.Siebel, H.Gasteiger, Analysis of Voltage Losses in PEM Water Electrolyzers with Low Platinum Group Metal Loadings, J. Electrochem. Soc. **165**(5) (2018) F305-F314.
[76] A.R.J. Kucernak, V.N. Naranammalpuram Sundaram, Nickel phosphide: the effect of phosphorus content on hydrogen evolution activity and corrosion resistance in acidic medium, J. Mater. Chem. A **2**(41) (2014) 17435-17445.
[77] O. Schmidt, A. Gambhir, I. Staffell, A. Hawkes, J. Nelson, S. Few, Future cost and performance of water electrolysis: An expert elicitation study, Int. J. Hydrogen Energy 42(52) (2017) 30470-30492.
[78] I. Flis-Kabulska, J. Flis, Electrodeposits of nickel with reduced graphene oxide (Ni/rGO) and their enhanced electroactivity towards hydrogen evolution in water electrolysis, Mater. Chem. Phys. **241** (2020) 122316.
[79] P. Li, H.C. Zeng, Sandwich-Like Nanocomposite of CoNiOx/Reduced Graphene Oxide for Enhanced Electrocatalytic Water Oxidation, Adv. Funct. Mater. **27**(13) (2017) 1606325.
[80] J. Guo, K. Zhang, A. Sun, Y. Zong, Z. Guo, Q. Liu, X. Zhang, Y. Xia, Enhanced hydrogen evolution of MoS2/RGO: vanadium, nitrogen dopants triggered new active sites and expanded interlayer, Inorg. Chem. Front. **5**(9) (2018) 2092-2099.
[81] Z. Deng, L. Li, W. Ding, K. Xiong, Z. Wei, Synthesized ultrathin MoS 2 nanosheets perpendicular to graphene for catalysis of hydrogen evolution reaction, Chemical communications (Cambridge, England) 51 (2014).
[82] Y. Li, H. Wang, L. Xie, Y. Liang, G. Hong, H. Dai, MoS2 Nanoparticles Grown on Graphene: An Advanced Catalyst for the Hydrogen Evolution Reaction, J. Am. Chem. Soc. 133(19) (2011) 7296-7299.
[83] P. Budania, P. Baine, J. Montgomery, C. McGeough, T. Cafolla, M. Modreanu, D. McNeill, N. Mitchell, G. Hughes, P. Hurley, Long-term stability of mechanically exfoliated MoS2 flakes, MRS Commun. **7**(4) (2017) 813-818.
[84] S.k. Balasingam, J.S. Lee, Y. Jun, Molybdenum diselenide/reduced graphene oxide based hybrid nanosheets for supercapacitor applications, Dalton Trans. 45 (2016).
[85] J. Guo, Y. Shi, X. Bai, X. Wang, T. Ma, Atomically thin MoSe2/graphene and WSe2/graphene nanosheets for the highly efficient oxygen reduction reaction, J. Mater. Chem. A 3(48) (2015) 24397-24404.
[86] J. Gusakova, X. Wang, L.L. Shiau, A. Krivosheeva, V. Shaposhnikov, V. Borisenko, V. Gusakov, B.K. Tay, Electronic Properties of Bulk and Monolayer TMDs: Theoretical Study Within DFT Framework (GVJ-2e Method), Phys. Status Solidi A 214(12) (2017) 1700218.
[87] H. Tang, K. Dou, C.-C. Kaun, Q. Kuang, S. Yang, MoSe2 nanosheets and their graphene hybrids: synthesis, characterization and hydrogen evolution reaction studies, Journal of Materials Chemistry A 2(2) (2014) 360-364.
[88] S. Sarker, J. Peters, X. Chen, B. Li, G. Chen, L. Yan, S.K. Richins, S. Das, M. Zhou, H. Luo, Engineering Molybdenum Diselenide and Its Reduced Graphene Oxide Hybrids for Efficient Electrocatalytic Hydrogen Evolution, ACS Applied Nano Materials 1(5) (2018) 2143-2152.
[89] M.D. Sharma, C. Mahala, M. Basu, 2D Thin Sheet Heterostructures of MoS2 on MoSe2 as Efficient Electrocatalyst for Hydrogen Evolution Reaction in Wide pH Range, Inorganic Chemistry 59(7) (2020) 4377-4388.
[90] P. Lindgren, G. Kastlunger, A.A. Peterson, A Challenge to the G ∼ 0 Interpretation of Hydrogen Evolution, ACS Catal. 10(1) (2020) 121-128.
[91] X. Yu, S. Ye, Recent advances in activity and durability enhancement of Pt/C catalytic cathode in PEMFC: Part II: Degradation mechanism and durability enhancement of carbon supported platinum catalyst, J. Power Sources 172(1) (2007) 145-154.
[92] N.Khan, Z.Hasan, S.Jhung, Beyond pristine metal-organic frameworks: Preparation and application of nanostructured, nanosized, and analogous MOFs, Coord. Chem. Rev. **376** (2018) 20-45.
[93] B. Zhu, R. Zou, Q. Xu, Metal–Organic Framework Based Catalysts for Hydrogen Evolution, Adv. Energy Mater. **8**(24) (2018) 1801193.

[94] F. Li, G.-F. Han, H.-J. Noh, J.-P. Jeon, I. Ahmad, S. Chen, C. Yang, Y. Bu, Z. Fu, Y. Lu, J.-B. Baek, Balancing hydrogen adsorption/desorption by orbital modulation for efficient hydrogen evolution catalysis, Nat. Commun. 10(1) (2019) 4060.
[95] Y. Zhu, W. Zhou, Z. Chen, Y. Chen, C. Su, M.O. Tadé, Z. Shao, SrNb0.1Co0.7Fe0.2O3−δ Perovskite as a Next-Generation Electrocatalyst for Oxygen Evolution in Alkaline Solution, Angew. Chem., Int. Ed. **54**(13) (2015) 3897-3901.
[96] D. Chen, C. Chen, Z.M. Baiyee, C. Shao, F. Ciucci, Nonstoichiometric Oxides as Low-Cost and Highly-Efficient Oxygen Reduction/Evolution Catalysts for Low-Temperature Electrochemical Devices, Chem. Rev. **115**(18) (2015) 9869-9921.
[97] J.-F. Qin, D. Du, W. Guan, X.-J. Bo, Y. Li, L.-P. Guo, Z. Su, Y. Wang, Y.-Q. Lan, H.-C. Zhou, Ultrastable Polymolybdate-Based Metal–Organic Frameworks as Highly Active Electrocatalysts for Hydrogen Generation from Water, J. Am. Chem. Soc. **137**(22) (2015) 7169-7177.
[98] B. Zhu, Y. Yang, Y. Guan, D. Xue, K. Cui, Construction of a cobalt-embedded nitrogen-doped carbon material with the desired porosity derived from the confined growth of MOFs within graphene aerogels as a superior catalyst towards HER and ORR, J. Mater. Chem. A **4**(40) (2016) 15536-15545.
[99] A.M. Dimiev, L.B. Alemany, J.M. Tour, Graphene Oxide. Origin of Acidity, Its Instability in Water, and a New Dynamic Structural Model, ACS Nano **7**(1) (2013) 576-588.
[100] A. García-Miranda Ferrari, D.A.C. Brownson, C. Banks, Investigating the Integrity of Graphene towards the Electrochemical Hydrogen Evolution Reaction (HER), Sci. Rep. **9**(1) (2019) 15961.
[101] A. García-Miranda Ferrari, D.A.C. Brownson, C. Banks, Investigating the Integrity of Graphene towards the Electrochemical Oxygen Evolution Reaction, ChemElectroChem **6**(21) (2019) 5446-5453.
[102] G. Kyriakou, M. Boucher, A. Jewell, E. Lewis, T. Lawton, A. Baber, H. Tierney, M. Flytzani-Stephanopoulos, E. Sykes, Isolated Metal Atom Geometries as a Strategy for Selective Heterogeneous Hydrogenations, Science **335**(6073) (2012) 1209.
[103] L. Fan, P. Liu, X. Yan, L. Gu, Z.Z. Yang, H. Yang, S. Qiu, X. Yao, Atomically isolated nickel species anchored on graphitized carbon for efficient hydrogen evolution electrocatalysis, Nat. Commun. **7** (2016) 10667.
[104] Y. Xue, B. Huang, Y. Yi, Y. Guo, Z. Zuo, Y. Li, Z. Jia, H. Liu, Y. Li, Anchoring zero valence single atoms of nickel and iron on graphdiyne for hydrogen evolution, Nature Communications 9(1) (2018) 1460.
[105] D. Bilczuk, O.G. Olvera, E. Asselin, Kinetic study of the dissolution of metallic nickel in sulphuric acid solutions in the presence of different oxidants, Can. J. Chem. Eng. **94**(10) (2016) 1872-1879.
[106] K.H. Kim, S.H. Lee, N.D. Nam, J.G. Kim, Effect of cobalt on the corrosion resistance of low alloy steel in sulfuric acid solution, Corros. Sci. 53(11) (2011) 3576-3587.
[107] S. Sathiyanarayanan, C. Jeyaprabha, S. Muralidharan, G. Venkatachari, Inhibition of iron corrosion in 0.5M sulphuric acid by metal cations, Appl. Surf. Sci. 252(23) (2006) 8107-8112.
[108] D.M. Dražić, L.Ž. Vorkapić, Inhibitory effects of manganeous, cadmium and zinc ions on hydrogen evolution reaction and corrosion of iron in sulphuric acid solutions, Corros. Sci. 18(10) (1978) 907-910.
[109] J.M. Gonçalves, T.A. Matias, K.C.F. Toledo, K. Araki, Chapter Six - Electrocatalytic materials design for oxygen evolution reaction, in: R. van Eldik, C.D. Hubbard (Eds.), Advances in Inorganic Chemistry, Academic Press2019, pp. 241-303.
[110] D.E. Schipper, Z. Zhao, H. Thirumalai, A.P. Leitner, S.L. Donaldson, A. Kumar, F. Qin, Z. Wang, L.C. Grabow, J. Bao, K.H. Whitmire, Effects of Catalyst Phase on the Hydrogen Evolution Reaction of Water Splitting: Preparation of Phase-Pure Films of FeP, Fe2P, and Fe3P and Their Relative Catalytic Activities, Chem. Mater. **30**(10) (2018) 3588-3598.
[111] K. Persson, "Materials Data on FeP (SG:62) by Materials Project", 2015.
[112] K. Persson, "Materials Data on Fe2P (SG:189) by Materials Project", 2016.
[113] K. Persson, Materials Data on Fe3P (SG:82) by Materials Project, 2016.
[114] J.Z. Wu, X. Chong, R. Zhou, Y. Jiang, J. Feng, Structure, stability, mechanical and electronic properties of Fe–P binary compounds by first-principles calculations, RSC Adv. **5**(100) (2015) 81943-81956.
[115] Z. Zhao, L. Liu, S.H. Zhang, T. Yu, F. Li, G. Yang, Phase diagram, stability and electronic properties of an Fe–P system under high pressure: a first principles study, RSC Adv. **7**(26) (2017) 15986-15991.
[116] E.J. Popczun, J.R. McKone, C.G. Read, A.J. Biacchi, A.M. Wiltrout, N.S. Lewis, R.E. Schaak, Nanostructured Nickel Phosphide as an Electrocatalyst for the Hydrogen Evolution Reaction, J. Am. Chem. Soc. **135**(25) (2013) 9267-9270.

[117] J.-S. Moon, J.-H. Jang, E.-G. Kim, Y.-H. Chung, S.J. Yoo, Y.-K. Lee, The nature of active sites of Ni2P electrocatalyst for hydrogen evolution reaction, J. Catal. **326** (2015) 92-99.
[118] Y. Liu, H. Yu, X. Quan, S. Chen, H. Zhao, Y. Zhang, Efficient and durable hydrogen evolution electrocatalyst based on nonmetallic nitrogen doped hexagonal carbon, Sci. Rep 4(1) (2014) 6843.
[119] Y. Zhu, M. Yuan, L. Deng, R. Ming, A. Zhang, M. Yang, B. Chai, Z. Ren, High-efficiency electrochemical hydrogen evolution based on the intermetallic Pt2Si compound prepared by magnetron-sputtering, RSC Adv. 7(3) (2017) 1553-1560.
[120] C. He, J. Tao, 2D Co6Mo6C Nanosheets as Robust Hydrogen Evolution Reaction Electrocatalyst, Advanced Sustainable Systems 2(2) (2018) 1700136.
[121] Y. Shi, B. Zhang, Recent advances in transition metal phosphide nanomaterials: synthesis and applications in hydrogen evolution reaction, Chem. Soc. Rev. **45**(6) (2016) 1529-1541.
[122] X. Wang, W. Li, D. Xiong, D.Y. Petrovykh, L. Liu, Bifunctional Nickel Phosphide Nanocatalysts Supported on Carbon Fiber Paper for Highly Efficient and Stable Overall Water Splitting, Advanced Functional Materials 26(23) (2016) 4067-4077.
[123] Y. Yan, B.Y. Xia, X. Ge, Z. Liu, A. Fisher, X. Wang, A Flexible Electrode Based on Iron Phosphide Nanotubes for Overall Water Splitting, Chemistry – A European Journal 21(50) (2015) 18062-18067.
[124] Y. Yan, X.R. Shi, M. Miao, T. He, Z.H. Dong, K. Zhan, J.H. Yang, B. Zhao, B.Y. Xia, Bio-inspired design of hierarchical FeP nanostructure arrays for the hydrogen evolution reaction, Nano Research 11(7) (2018) 3537-3547.
[125] Q. Yang, R. Zhang, W. Wang, P. Zhou, L. Wang, T. Chen, H. Xu, L. Zheng, Metal organic framework (MOF) derived iron phosphide as a highly stable and efficient catalyst for hydrogen evolution, Sustainable Energy & Fuels 3(11) (2019) 3078-3084.
[126] C.C.L. McCrory, S. Jung, J.C. Peters, T.F. Jaramillo, Benchmarking Heterogeneous Electrocatalysts for the Oxygen Evolution Reaction, J. Am. Chem. Soc. **135**(45) (2013) 16977-16987.
[127] C.H. Lee, J. Suntivich, K. May, E.E. Perry, Y. Shao-Horn, Synthesis and Activities of Rutile IrO2 and RuO2 Nanoparticles for Oxygen Evolution in Acid and Alkaline Solutions, J. Phys. Chem. Lett. **3**(3) (2012) 399-404.
[128] Y. Lin, Z. Tian, L. Zhang, J. Ma, Z. Jiang, B.J. Deibert, R. Ge, L. Chen, Chromium-ruthenium oxide solid solution electrocatalyst for highly efficient oxygen evolution reaction in acidic media, Nature Communications 10(1) (2019) 162.
[129] D. Böhm, M. Beetz, M. Schuster, K. Peters, A.G. Hufnagel, M. Döblinger, B. Böller, T. Bein, D. Fattakhova-Rohlfing, Efficient OER Catalyst with Low Ir Volume Density Obtained by Homogeneous Deposition of Iridium Oxide Nanoparticles on Macroporous Antimony-Doped Tin Oxide Support, Advanced Functional Materials 30(1) (2020) 1906670.
[130] Z. Li, X. Wang, X. Wang, Y. Lin, A. Meng, L. Yang, Q. Li, Mn-Cd-S@amorphous-Ni3S2 hybrid catalyst with enhanced photocatalytic property for hydrogen production and electrocatalytic OER, Applied Surface Science 491 (2019) 799-806.
[131] F. Maillard, W. O. Silva, L. Castanheira, L. Dubau, F.H.B. Lima, Carbon Corrosion in Proton-Exchange Membrane Fuel Cells: Spectrometric Evidence for Pt-Catalysed Decarboxylation at Anode-Relevant Potentials, ChemPhysChem 20(22) (2019) 3106-3111.
[132] B.-S. Lee, S.H. Ahn, H.-Y. Park, I. Choi, S.J. Yoo, H.-J. Kim, D. Henkensmeier, J.Y. Kim, S. Park, S.W. Nam, K.-Y. Lee, J.H. Jang, Development of electrodeposited IrO2 electrodes as anodes in polymer electrolyte membrane water electrolysis, Applied Catalysis B: Environmental 179 (2015) 285-291.
[133] C.V. Pham, M. Bühler, J. Knöppel, M. Bierling, D. Seeberger, D. Escalera-López, K.J.J. Mayrhofer, S. Cherevko, S. Thiele, IrO2 coated TiO2 core-shell microparticles advance performance of low loading proton exchange membrane water electrolyzers, Applied Catalysis B: Environmental 269 (2020) 118762.
[134] M. Huynh, C. Shi, S.J.L. Billinge, D.G. Nocera, Nature of Activated Manganese Oxide for Oxygen Evolution, J. Am. Chem. Soc. **137**(47) (2015) 14887-14904.
[135] M. Huynh, D.K. Bediako, D.G. Nocera, A Functionally Stable Manganese Oxide Oxygen Evolution Catalyst in Acid, J. Am. Chem. Soc. **136**(16) (2014) 6002-6010.
[136] M.S. Burke, L.J. Enman, A.S. Batchellor, S. Zou, S.W. Boettcher, Oxygen Evolution Reaction Electrocatalysis on Transition Metal Oxides and (Oxy)hydroxides: Activity Trends and Design Principles, Chem. Mater. **27**(22) (2015) 7549-7558.
[137] A.L. Strickler, M.a. Escudero-Escribano, T.F. Jaramillo, Core–Shell Au@Metal-Oxide Nanoparticle Electrocatalysts for Enhanced Oxygen Evolution, Nano Letters 17(10) (2017) 6040-6046.

[138] D.M. Prices, Daily Metal Spot Prices, 2020.
[139] W. Stumm, Reactivity at the mineral-water interface: dissolution and inhibition, Colloids Surf., A **120**(1) (1997) 143-166.
[140] R. Frydendal, E.A. Paoli, I. Chorkendorff, J. Rossmeisl, I.E.L. Stephens, Toward an Active and Stable Catalyst for Oxygen Evolution in Acidic Media: Ti-Stabilized MnO2, Adv. Energy Mater. **5**(22) (2015) 1500991.
[141] M. Huynh, T. Ozel, C. Liu, E.C. Lau, D.G. Nocera, Design of template-stabilized active and earth-abundant oxygen evolution catalysts in acid, Chem. Sci. **8**(7) (2017) 4779-4794.
[142] M. Huynh, T. Ozel, C. Liu, E.C. Lau, D.G. Nocera, Design of template-stabilized active and earth-abundant oxygen evolution catalysts in acid, Chemical Science 8(7) (2017) 4779-4794.
[143] B. Hammer, J. Nørskov, Theoretical surface science and catalysis—calculations and concepts, Advances in Catalysis, Academic Press2000, pp. 71-129.
[144] P.P. Patel, M.K. Datta, O.I. Velikokhatnyi, R. Kuruba, K. Damodaran, P. Jampani, B. Gattu, P.M. Shanthi, S.S. Damle, P.N. Kumta, Noble metal-free bifunctional oxygen evolution and oxygen reduction acidic media electro-catalysts, Sci. Rep. **6** (2016) 28367.
[145] L. Chen, J. Chang, Y. Zhang, Z. Gao, D. Wu, F. Xu, F. Guo, X. Jiang, Fluorine anion-enriched nickel hydroxyl oxide as an efficient oxygen evolution reaction electrocatalyst, Chem. Commun. **55**(23) (2019) 3406-3409.
[146] P.Chen, T.Zhou, S.Wang, N.Zhang, Y.Tong, H.Ju, W.Chu, C.Wu, Y.Xie, Dynamic Migration of Surface Fluorine Anions on Cobalt-Based Materials to Achieve Enhanced Oxygen Evolution Catalysis, Angew. Chem., Int. Ed. **57**(47) (2018) 15471-15475.
[147] X. Bai, Q. Wang, G. Xu, Y. Ning, K. Huang, F. He, Z. Wu, J. Zhang, Phosphorus and Fluorine Co-Doping Induced Enhancement of Oxygen Evolution Reaction in Bimetallic Nitride Nanorods Arrays: Ionic Liquid-Driven and Mechanism Clarification, Chem. Eur. J. **23**(66) (2017) 16862-16870.
[148] S.D. Ghadge, P.P. Patel, M.K. Datta, O.I. Velikokhatnyi, R. Kuruba, P.M. Shanthi, P.N. Kumta, Fluorine substituted (Mn,Ir)O2:F high performance solid solution oxygen evolution reaction electro-catalysts for PEM water electrolysis, RSC Adv. **7**(28) (2017) 17311-17324.
[149] K. Kadakia, M.K. Datta, O.I. Velikokhatnyi, P. Jampani, S.K. Park, S.J. Chung, P.N. Kumta, High performance fluorine doped (Sn,Ru)O2 oxygen evolution reaction electro-catalysts for proton exchange membrane based water electrolysis, J. Power Sources **245** (2014) 362-370.
[150] K. Swaminathan, O. Sreedharan, Potentiometric determination of stabilities of NiSb2O4 and NiSb2O6, J. Alloys Compd. **292**(1) (1999) 100-106.
[151] I.A. Moreno-Hernandez, C.A. MacFarland, C.G. Read, K.M. Papadantonakis, B.S. Brunschwig, E. Lewis, Crystalline nickel manganese antimonate as a stable water-oxidation catalyst in aqueous 1.0 M H2SO4, Energy Environ. Sci. **10**(10) (2017) 2103-2108.
[152] R.W. Hewitt, N. Winograd, Investigation of the oxidation of polycrystalline lead by XPS and SIMS, Surface Science 78(1) (1978) 1-14.
[153] C. Wei, W. Wu, H. Li, X. Lin, T. Wu, Y. Zhang, Q. Xu, L. Zhang, Y. Zhu, X. Yang, Z. Liu, Q. Xu, Atomic Plane-Vacancy Engineering of Transition-Metal Dichalcogenides with Enhanced Hydrogen Evolution Capability, ACS Appl. Energy Mater. **11**(28) (2019) 25264-25270.
[154] W. Li, D. Xiong, X. Gao, L. Liu, The oxygen evolution reaction enabled by transition metal phosphide and chalcogenide pre-catalysts with dynamic changes, Chem. Commun. **55**(60) (2019) 8744-8763.
[155] J.Z. Wu, M. Liu, K. Chatterjee, K.P. Hackenberg, J. Shen, X. Zou, Y. Yan, J. Gu, Y. Yang, J. Lou, P.M. Ajayan, Exfoliated 2D Transition Metal Disulfides for Enhanced Electrocatalysis of Oxygen Evolution Reaction in Acidic Medium, Adv. Mater. Interfaces **3**(9) (2016) 1500669.
[156] J.S. Mondschein, K. Kumar, C.F. Holder, K. Seth, H.Y. Kim, R.E. Schaak, Intermetallic Ni2Ta Electrocatalyst for the Oxygen Evolution Reaction in Highly Acidic Electrolytes, Inorg. Chem. **57**(10) (2018) 6010-6015.
[157] W. Luo, J. Gan, Z. Huang, W. Chen, G. Qian, X. Zhou, X. Duan, Boosting HER Performance of Pt-Based Catalysts Immobilized on Functionalized Vulcan Carbon by Atomic Layer Deposition, Frontiers in Materials 6(251) (2019).
[158] H. Li, C. Chen, D. Yan, Y. Wang, R. Chen, Y. Zou, S. Wang, Interfacial effects in supported catalysts for electrocatalysis, Journal of Materials Chemistry A 7(41) (2019) 23432-23450.
[159] T.R. Hellstern, J. Kibsgaard, C. Tsai, D.W. Palm, L.A. King, F. Abild-Pedersen, T.F. Jaramillo, Investigating Catalyst–Support Interactions To Improve the Hydrogen Evolution Reaction Activity of Thiomolybdate [Mo3S13]2– Nanoclusters, ACS Catalysis 7(10) (2017) 7126-7130.

[160] A.P. Murthy, J. Madhavan, K. Murugan, Recent advances in hydrogen evolution reaction catalysts on carbon/carbon-based supports in acid media, J. Power Sources **398** (2018) 9-26.
[161] C.W. Foster, R.O. Kadara, C. Banks, Fundamentals of Screen-Printing Electrochemical Architectures, in: C.E. Banks, C.W. Foster, R.O. Kadara (Eds.), Screen-Printing Electrochemical Architectures, Springer International Publishing, Cham, 2016, pp. 13-23.
[162] S. Rowley-Neale, C.W. Foster, G. Smith, D.A.C. Brownson, C. Banks, Mass-producible 2D-MoSe2 bulk modified screen-printed electrodes provide significant electrocatalytic performances towards the hydrogen evolution reaction, Sustainable Energy Fuels 1(1) (2017) 74-83.
[163] S.Rowley-Neale, M.Ratova, L.Fugita, G.Smith, A.Gaffar, J.Kulczyk-Malecka, P.Kelly, C.Banks, Magnetron Sputter-Coated Nanoparticle MoS2 Supported on Nanocarbon: A Highly Efficient Electrocatalyst toward the Hydrogen Evolution Reaction, ACS Omega 3 (2018).
[164] S. Rowley-Neale, G. Smith, C. Banks, Mass-Producible 2D-MoS2-Impregnated Screen-Printed Electrodes That Demonstrate Efficient Electrocatalysis toward the Oxygen Reduction Reaction, ACS Appl. Mater. Interfaces 9(27) (2017) 22539-22548.
[165] W. Wang, S. Chen, J. Li, W. Wang, Fabrication of catalyst coated membrane with screen printing method in a proton exchange membrane fuel cell, Int. J. Hydrogen Energy **40**(13) (2015) 4649-4658.
[166] C. Hao, H. Lv, C. Mi, Y.-I. Song, J. Ma, Investigation of Mesoporous Niobium-Doped TiO2 as an Oxygen Evolution Catalyst Support in an SPE Water Electrolyzer, ACS Sustainable Chem. Eng. **4**(3) (2016) 746-756.
[167] S.Siracusano, N.V. Dijk, R.Backhouse, L.Merlo, V.Baglio, A.Aricò, Degradation issues of PEM electrolysis MEAs, Renewable Energy **123** (2018) 52-57.
[168] P. Millet, N. Mbemba, S.A. Grigoriev, V.N. Fateev, A. Aukauloo, C. Etiévant, Electrochemical performances of PEM water electrolysis cells and perspectives, International Journal of Hydrogen Energy 36(6) (2011) 4134-4142.
[169] P. Mazúr, J. Polonský, M. Paidar, K. Bouzek, Non-conductive TiO2 as the anode catalyst support for PEM water electrolysis, Int. J. Hydrogen Energy **37**(17) (2012) 12081-12088.
[170] W. Hu, S. Chen, Q. Xia, IrO2/Nb–TiO2 electrocatalyst for oxygen evolution reaction in acidic medium, Int. J. Hydrogen Energy **39**(13) (2014) 6967-6976.
[171] V. Ávila-Vázquez, J. Cruz, M. Galván-valencia, J. Ledesma-García, L.G. Arriaga, C. Guzmán, S. Duron-Torres, Electrochemical Study of Sb-Doped SnO2 Supports on the Oxygen Evolution Reaction: Effect of Synthesis Annealing Time, Int. J. Electrochem. Sci. **8** (2013) 10586-10600.
[172] A. Marshall, R. Haverkamp, Electrocatalytic activity of IrO 2–RuO 2 supported on Sb-doped SnO 2 nanoparticles, Electrochimica Acta - ELECTROCHIM ACTA 55 (2010) 1978-1984.
[173] H.-s. Oh, H. Nong, T. Reier, M. Gliech, P. Strasser, Oxide-supported Ir nanodendrites with high activity and durability for the oxygen evolution reaction in acid PEM water electrolyzers, Chem. Sci. 6 (2015).
[174] M. Thomassen, T. Mokkelbost, E. Sheridan, A. Lind, Supported Nanostructured Ir and IrRu Electrocatalysts for Oxygen Evolution in PEM Electrolysers, 2011.
[175] L. Zhao, Q. Cao, A. Wang, J. Duan, W. Zhou, Y. Sang, H. Liu, Iron oxide embedded titania nanowires – An active and stable electrocatalyst for oxygen evolution in acidic media, Nano Energy 45 (2018) 118-126.
[176] J. Xu, Q. Li, M.K. Hansen, E. Christensen, A.L. Tomás García, G. Liu, X. Wang, N.J. Bjerrum, Antimony doped tin oxides and their composites with tin pyrophosphates as catalyst supports for oxygen evolution reaction in proton exchange membrane water electrolysis, International Journal of Hydrogen Energy 37(24) (2012) 18629-18640.
[177] K.S. Huh, H.J. Hong, E.W. Lee, S.Y. Park, C.W. Jeon, S.H. Lee, Properties of Transparent Conducting ATO Films Deposited by RF Magnetron Sputtering, Molecular Crystals and Liquid Crystals 532(1) (2010) 65/[481]-71/[487].
[178] B. Rodríguez-García, Á. Reyes-Carmona, I. Jiménez-Morales, M. Blasco-Ahicart, S. Cavaliere, M. Dupont, D. Jones, J. Rozière, J.R. Galán-Mascarós, F. Jaouen, Cobalt hexacyanoferrate supported on Sb-doped SnO2 as a non-noble catalyst for oxygen evolution in acidic medium, Sustainable Energy & Fuels 2(3) (2018) 589-597.
[179] S. Zhao, A. Stocks, B. Rasimick, K. More, H. Xu, Highly Active, Durable Dispersed Iridium Nanocatalysts for PEM Water Electrolyzers, Journal of The Electrochemical Society 165 (2018) F82-F89.
[180] S. Geiger, O. Kasian, A.M. Mingers, K.J.J. Mayrhofer, S. Cherevko, Stability limits of tin-based electrocatalyst supports, Scientific reports 7(1) (2017) 4595-4595.
[181] G. Liu, J. Xu, Y. Wang, X. Wang, An oxygen evolution catalyst on an antimony doped tin oxide nanowire structured support for proton exchange membrane liquid water electrolysis, Journal of Materials Chemistry A 3(41) (2015) 20791-20800.

[182] N. Lindahl, E. Zamburlini, L. Feng, H. Grönbeck, M. Escudero-Escribano, I.E.L. Stephens, I. Chorkendorff, C. Langhammer, B. Wickman, High Specific and Mass Activity for the Oxygen Reduction Reaction for Thin Film Catalysts of Sputtered Pt3Y, Advanced Materials Interfaces 4(13) (2017) 1700311.
[183] C. Wei, R.R. Rao, J. Peng, B. Huang, I.E.L. Stephens, M. Risch, Z.J. Xu, Y. Shao-Horn, Recommended Practices and Benchmark Activity for Hydrogen and Oxygen Electrocatalysis in Water Splitting and Fuel Cells, Advanced Materials 31(31) (2019) 1806296.
[184] Y. Sugita, T. Tamaki, H. Kuroki, T. Yamaguchi, Connected iridium nanoparticle catalysts coated onto silica with high density for oxygen evolution in polymer electrolyte water electrolysis, Nanoscale Advances 2(1) (2020) 171-175.
[185] A.H. Ghanim, J.G. Koonce, B. Hasa, A.M. Rassoolkhani, W. Cheng, D.W. Peate, J. Lee, S. Mubeen, Low-Loading of Pt Nanoparticles on 3D Carbon Foam Support for Highly Active and Stable Hydrogen Production, Frontiers in chemistry 6 (2018) 523-523.
[186] J. Lai, B. Huang, Y. Chao, X. Chen, S. Guo, Strongly Coupled Nickel–Cobalt Nitrides/Carbon Hybrid Nanocages with Pt-Like Activity for Hydrogen Evolution Catalysis, Advanced Materials 31(2) (2019) 1805541.
[187] T. Wang, Y. Guo, Z. Zhou, C. Xinghua, J. Zheng, X. Li, Ni-Mo Nanocatalysts on N-Doped Graphite Nanotubes for Highly Efficient Electrochemical Hydrogen Evolution in Acid, ACS Nano 10 (2016).
[188] J.K. Das, A.K. Samantara, A.K. Nayak, D. Pradhan, J.N. Behera, VS2: an efficient catalyst for an electrochemical hydrogen evolution reaction in an acidic medium, Dalton Trans. 47(39) (2018) 13792-13799.
[189] M. Chhetri, S. Sultan, C.N.R. Rao, Electrocatalytic hydrogen evolution reaction activity comparable to platinum exhibited by the Ni/Ni(OH)/graphite electrode, Proc. Natl. Acad. Sci. U.S.A. 114(34) (2017) 8986.
[190] O. Kasian, S. Geiger, K.J.J. Mayrhofer, S. Cherevko, Electrochemical On-line ICP-MS in Electrocatalysis Research, The Chemical Record 19(10) (2019) 2130-2142.
[191] S. Siracusano, N. Hodnik, P. Jovanovic, F. Ruiz-Zepeda, M. Šala, V. Baglio, A.S. Aricò, New insights into the stability of a high performance nanostructured catalyst for sustainable water electrolysis, Nano Energy 40 (2017) 618-632.
[192] I. Spanos, A.A. Auer, S. Neugebauer, X. Deng, H. Tüysüz, R. Schlögl, Standardized Benchmarking of Water Splitting Catalysts in a Combined Electrochemical Flow Cell/Inductively Coupled Plasma–Optical Emission Spectrometry (ICP-OES) Setup, ACS Catalysis 7(6) (2017) 3768-3778.
[193] L. Nguyen, F.F. Tao, Y. Tang, J. Dou, X.-J. Bao, Understanding Catalyst Surfaces during Catalysis through Near Ambient Pressure X-ray Photoelectron Spectroscopy, Chemical Reviews 119(12) (2019) 6822-6905.
[194] L. Zhong, D. Chen, S. Zafeiratos, A mini review of in situ near-ambient pressure XPS studies on non-noble, late transition metal catalysts, Catalysis Science & Technology 9(15) (2019) 3851-3867.
[195] A.M. Motin, T. Haunold, A.V. Bukhtiyarov, A. Bera, C. Rameshan, G. Rupprechter, Surface science approach to Pt/carbon model catalysts: XPS, STM and microreactor studies, Applied Surface Science 440 (2018) 680-687.
[196] K. Friedrich, P. Lettenmeier, A. Ansar, L. Wang, A. Gago, Achieving Cost Reduction in PEM Electrolysis by Material Development, 2017.
[197] P. Liu, J. Zhu, J. Zhang, P. Xi, K. Tao, D. Gao, D. Xue, P Dopants Triggered New Basal Plane Active Sites and Enlarged Interlayer Spacing in MoS2 Nanosheets toward Electrocatalytic Hydrogen Evolution, ACS Energy Lett. **2**(4) (2017) 745-752.
[198] P.S. Adarakatti, M. Mahanthappa, J.P. Hughes, S. Rowley-Neale, G. Smith, S. Ashoka, C. Banks, MoS2-graphene-CuNi2S4 nanocomposite an efficient electrocatalyst for the hydrogen evolution reaction, Int. J. Hydrogen Energy **44**(31) (2019) 16069-16078.
[199] Z. Wu, B. Fang, Z. Wang, C. Wang, Z. Liu, F. Liu, W. Wang, A. Alfantazi, D. Wang, D.P. Wilkinson, MoS2 Nanosheets: A Designed Structure with High Active Site Density for the Hydrogen Evolution Reaction, ACS Catal. **3**(9) (2013) 2101-2107.
[200] G. Hu, J. Li, P. Liu, X. Zhu, X.W. Li, R.N. Ali, B. Xiang, Enhanced electrocatalytic activity of WO3@NPRGO composite in a hydrogen evolution reaction, Appl. Surf. Sci. **463** (2019) 275-282.
[201] T.H. Wondimu, B. Chen, D.M. Kabtamu, H. Chen, A.W. Bayeh, H. Huang, C. Wang, Highly efficient and durable phosphine reduced iron-doped tungsten oxide/reduced graphene oxide nanocomposites for the hydrogen evolution reaction, Int. J. Hydrogen Energy **43**(13) (2018) 6481-6490.
[202] S. Mao, Z. Wen, S. Ci, X. Guo, K. Ostrikov, J.Y.C. Chen, Perpendicularly Oriented MoSe2/Graphene Nanosheets as Advanced Electrocatalysts for Hydrogen Evolution, Small **11**(4) (2015) 414-419.

[203] Z. Lei, S. Xu, B.-D. Wu, Ultra-thin and porous MoSe2 nanosheets: facile preparation and enhanced electrocatalytic activity towards the hydrogen evolution reaction, Phys. Chem. Chem. Phys. **18**(1) (2016) 70-74.
[204] Y. Li, S. Niu, D. Rakov, Y. Wang, M. Cabán-Acevedo, S. Zheng, B. Song, P. Xu, Metal organic framework-derived CoPS/N-doped carbon for efficient electrocatalytic hydrogen evolution, Nanoscale **10**(15) (2018) 7291-7297.
[205] J. Hao, W. Yang, A. Zhang, J. Tang, Metal–organic frameworks derived CoxFe1−xP nanocubes for electrochemical hydrogen evolution, Nanoscale **7**(25) (2015) 11055-11062.
[206] W. Zhou, J. Lu, K. Zhou, L. Yang, Y. Ke, Z. Tang, S. Chen, CoSe2 nanoparticles embedded defective carbon nanotubes derived from MOFs as efficient electrocatalyst for hydrogen evolution reaction, Nano Energy **28** (2016) 143-150.
[207] H.B. Wu, B.Y. Xia, L. Yu, X. Yu, X. Lou, Porous molybdenum carbide nano-octahedrons synthesized via confined carburization in metal-organic frameworks for efficient hydrogen production, Nat. Commun. **6** (2015) 6512.
[208] M. Xu, L. Han, Y. Han, Y. Yu, J. Zhai, S. Dong, Porous CoP concave polyhedron electrocatalysts synthesized from metal–organic frameworks with enhanced electrochemical properties for hydrogen evolution, J. Mater. Chem. A **3**(43) (2015) 21471-21477.
[209] A. Sumboja, T. An, H.Y. Goh, M. Lübke, D.P. Howard, Y. Xu, A.D. Handoko, Y. Zong, Z. Liu, One-Step Facile Synthesis of Cobalt Phosphides for Hydrogen Evolution Reaction Catalysts in Acidic and Alkaline Medium, ACS Appl. Mater. Interfaces **10**(18) (2018) 15673-15680.
[210] F. Wang, Xang, B. Dong, X. Yu, H. Xue, L. Feng, A FeP powder electrocatalyst for the hydrogen evolution reaction, Electrochem. Commun. 92 (2018) 33-38.
[211] Y. Xu, R. Wu, J. Zhang, Y. Shi, B. Zhang, Anion-exchange synthesis of nanoporous FeP nanosheets as electrocatalysts for hydrogen evolution reaction, Chem. Commun. **49**(59) (2013) 6656-6658.
[212] Z. Huang, J. Liu, Z. Xiao, H. Fu, W. Fan, B. Xu, B. Dong, D. Liu, F. Dai, D. Sun, A MOF-derived coral-like NiSe@NC nanohybrid: an efficient electrocatalyst for the hydrogen evolution reaction at all pH values, Nanoscale **10**(48) (2018) 22758-22765.
[213] K.Yan, J.Chi, J.Xie, B.Dong, Z.Liu, W.Gao, J.Lin, Y.Chai, C.Liu, Mesoporous Ag-doped Co3O4 nanowire arrays supported on FTO as efficient electrocatalysts for oxygen evolution reaction in acidic media, Renewable Energy **119** (2018) 54-61.
[214] K. Mamtani, D. Jain, D. Dogu, V. Gustin, S. Gunduz, A.C. Co, U.S. Ozkan, Insights into oxygen reduction reaction (ORR) and oxygen evolution reaction (OER) active sites for nitrogen-doped carbon nanostructures (CNx) in acidic media, Appl. Catal., B **220** (2018) 88-97.
[215] W. Li, H. Chen, X. Long, F. Wu, Y. Wu, J. Yan, C. Zhang, Oxygen evolution reaction on lead–bismuth alloys in sulfuric acid solution, J. Power Sources **158**(2) (2006) 902-907.
[216] J.S. Mondschein, J.F. Callejas, C.G. Read, J.Y.C. Chen, C.F. Holder, C.K. Badding, R.E. Schaak, Crystalline Cobalt Oxide Films for Sustained Electrocatalytic Oxygen Evolution under Strongly Acidic Conditions, Chem. Mater. **29**(3) (2017) 950-957.

Electronic Supporting Information (ESI) for the following publication:

Polymer Electrolyte Electrolysis: A Review of the Activity and Stability of Non-Precious Metal Hydrogen Evolution Reaction and Oxygen Evolution Reaction Catalysts

Hughes, J.P.[1,2], Clipsham, J.[3], Chavushoglu, H.[1,2], Rowley-Neale, S.J.[1,2*] and Banks, C.E.[1,2*]

[1]: Faculty of Science and Engineering, Manchester Metropolitan University, Chester Street, Manchester M1 5GD, UK.

[2]: Manchester Fuel Cell Innovation Centre, Manchester Metropolitan University, Chester Street, Manchester M1 5GD, UK.

[3]: European Marine Energy Centre, The Charles Clouston Building, ORIC, Back Rd, Orkney KW16 3AW, UK

*To whom correspondence should be addressed.

Email: c.banks@mmu.ac.uk; Tel: ++(0)1612471196; Fax: ++(0)1612476831

Website: www.craigbanksresearch.com

Table 1. Summary of current literature pertaining to HER catalysts.

Catalyst	Supporting electrode	Electrolyte	Stability in acidic media	Deposition technique	Loading	HER onset (V)	Current Density at 150mV (mA/cm^{-2})	Tafel value (mV dec^{-1})	Ref
P-MoS_2	GC	0.5 M H_2SO_4	20h at −100 mV (*vs.* RHE)	Drop-cast	0.32 mg cm^{-2}	−0.02 (*vs.* RHE)	-	34	[197]
Li-MoS_2	CF	0.5 M H_2SO_4	2h at −118 mV (*vs.* RHE)	Chemical growth	3.4-3.9 mg cm^{-2}	−0.10 (*vs.* RHE)	*ca.* −50	62	[70]
MoS_2-g-$CuNi_2S_4$	SPE	0.5 M H_2SO_4	1000 cycles (0.2 to −0.2 V) (*vs.* RHE)	Drop cast	0.30 mg cm^{-2}	−0.05 (*vs.* RHE)	-	29	[198]
MoS_2 NSs	GC	0.5 M H_2SO_4	1000 cycles (−0.3 to 0.1 V) (*vs.* RHE)	Drop cast	0.29 mg cm^{-2}	−0.04 (*vs.* RHE)	−4.56	68	[199]
V, N – MoS_2/rGO	GC	0.5 M H_2SO_4	20h at 90mV (*vs.* RHE)	Drop cast	-	−0.03 (*vs.* RHE)	*ca.* 95	41	[80]
2D-MoS_2	SPE	0.5 H2SO4	1000 cycles (0.0 to −0.8 V) (*vs.* RHE)	Drop Cast	0.0013 mg cm^{-2}	−0.19 (*vs.* RHE)	−0.25	92	[53]
W_xC/NG	GC	0.5 M H_2SO_4	10000 cycles at 100mV s^{-1} (*vs.* RHE)	Drop cast	-	−0.08 (*vs.* RHE)	−30	45.9	[52]
rGO/WS_2/WO_3	GC	0.5 M H_2SO_4	1000 cycles (−1.0 to 0 V) (*vs.* RHE)	Drop casting	-	−0.09 (*vs.* RHE)	−5	37	[200]
Fe-WO_XP/rGO	GC	0.5 M H_2SO_4	8h at 10 mA cm^{-2}	Drop casting	-	−0.075 (*vs.* RHE)	−74	41.9	[201]
2D-WS_2	SPE	0.5 M H_2SO_4	1000 cycles (0.2 to −1.3 V) (*vs.* RHE)	Screen printing	-	−0.21 (*vs.* RHE)	−0.4	51.1	[41]
2D-$MoSe_2$	SPE	0.5 M H_2SO_4	1000 scans (0.0 to −1.4 V) (*vs.* RHE)	Screen printing	20%	−0.18 (*vs.* RHE)	−0.2	63	[162]
$MoSe_2$/GN	GC	0.5 M H_2SO_4	6000s (0.2 to −0.4 V) (*vs.* RHE)	CVD	-	−0.05 (*vs.* RHE)	−9	61	[202]
$MoSe_2$/rGO	GC	0.5 M H_2SO_4	2h at 200mV (*vs.* RHE)	Drop casting	0.16 mg cm^{-2}	−0.05 (*vs.* RHE)	−1	69	[87]
$MoSe_2$ NSs	GC	0.5 M H_2SO_4	1000 cycles (0.1 to −0.3 V) (*vs.* RHE)	Drop casting	-	−0.08 (*vs.* RHE)	−2.6	80	[203]

Co-N-GA	GC	0.5 M H_2SO_4	5000 cycles (−0.25 to 0.1 V) (*vs.* RHE)	Drop casting	0.28 mg cm^{-2}	−0.03 (*vs.* RHE)	−76	33	[98]
A-Ni-C	GC	0.5 M H_2SO_4	4h at −200mV (*vs.* RHE)	Drop casting	0.283 mg cm^{-2}	−0.03 (*vs.* RHE)	-	41	[103]
CoPS/N-S	GC	0.5 M H_2SO_4	16h at 80mV (*vs.* RHE)	Drop casting	0.17 mg cm^{-2}	−0.045 (*vs.* RHE)	−10	68	[204]
$Co_{0.59}Fe_{0.41}P$	GC	0.5 M H_2SO_4	20h at 72mV (vs. RHE)	Drop casting	0.35 mg cm^{-2}	−0.03 (*vs.* RHE)	−38	52	[205]
Ni_2P–CoP	GC	0.5 M H_2SO_4	14h at 0.14 V (vs. RHE)	Drop casting	0.357 mg cm^{-2}	−0.06 (*vs.* RHE)	−71	64	[206]
MoC_x	GC	0.5 M H_2SO_4	10h at 170 mV (vs. RHE)	Drop casting	0.80 mg cm^{-2}	−0.04 (*vs.* RHE)	−12	53	[207]
CoP CPHs	GC	0.5 M H_2SO_4	>12h at 130 mV (vs. RHE)	Drop casting	0.35 mg cm^{-2}	−0.06 (*vs.* RHE)	−17	51	[208]
CP@Ni-P	CF	0.5 M H_2SO_4	150h at 10 mA cm^{-2} (vs. RHE)	Chemical synthesis	0.30 mg cm^{-2}	−0.05 (*vs.* RHE)	−20	58.8	[122]
Ni_2P	GC	0.5 M H_2SO_4	500 cycles (0 to −0.25 V) (vs. RHE)	Drop casting	-	−0.03 (*vs.* RHE)	−14	75	[117]
Co-P	GC	0.5 M H_2SO_4	13h at 10 mA cm^{-2} (vs. RHE)	Drop casting	0.20 mg cm^{-2}	−0.04 (*vs.* RHE)	−8	56	[209]
Fe_2P	FTO	0.5 M H_2SO_4	20h at 120 mV (vs. RHE)	CVD	-	−0.05 (*vs.* RHE)	−76	66	[110]
Fe_3P	FTO	0.5 M H_2SO_4	20h at 120 mV (vs. RHE)	CVD	-	−0.02 (*vs.* RHE)	-	57	[110]
FeP	GC	0.5 M H_2SO_4	60h at 50 mA cm^{-2} (vs. RHE)	Drop casting	0.28 mg cm^{-2}	−0.025 (*vs.* RHE)	−91	57	[210]
FeP NSs	GC	0.5 M H_2SO_4	-	Drop casting	0.28 mg cm^{-2}	−0.09 (*vs.* RHE)	−4	67	[211]
NiSe@NC	GC	0.5 M H_2SO_4	12h at 156 mV (vs. RHE)	Drop casting	0.35 mg cm^{-2}	−0.05 (*vs.* RHE)	−16	53.3	[212]

: CPH; concave polyhedron GC; Glassy Carbon RHE; Reversible hydrogen electrode NF; Nickel foam NS: Nanosheet A: Activated rGO; Reduced graphene oxide GA; Graphene aerogel CVD; Chemical vapor deposition G; Graphene CF; Carbon filter FTO; Fluorine doped Tin Oxide

Table 2. Summary of current optimal anodic electrocatalysts

Catalyst	Supporting electrode	Electrolyte	Stability in acidic media	Deposition technique	Loading	OER onset (V)	Over potential (mV) to reach 10 $mAcm^{-2}$	Tafel value ($mV\ dec^{-1}$)	Ref
Ni_2Ta	PVC coated Sn-Cu wire	0.5 M H_2SO_4	70+h at 10 $mAcm^{-2}$	Ag paint	-	+1.75 (*vs.* RHE)	570 (*vs.* RHE)	-	[156]
Fe_2Ta	PVC coated Sn-Cu wire	0.5 M H_2SO_4	-	Ag paint	-	+1.74 (*vs.* RHE)	770 (*vs.* RHE)	-	[156]
Co_2Ta	PVC coated Sn-Cu wire	0.5 M H_2SO_4	-	Ag paint	-	+1.64 (*vs.* RHE)	600 (*vs.* RHE)	-	[156]
Ag-Co_3O_4	FTO	0.5 M H_2SO_4	12h at 1.6 V (*vs.* RHE)	Electrodeposition/hydrothermal	-	+1.65 (*vs.* RHE)	680 (*vs.* RHE)	219	[213]
Ag-$Ni_{(1)}$ $Co_3O_{4(2)}$	FTO	0.5 M H_2SO_4	-	Electrodeposition/hydrothermal	-	+1.71 (*vs.* RHE)	730 (*vs.* RHE)	112	[213]
CN_x	GC	0.1 M $HClO_4$	-	Drop casting	800 µg cm^{-2}	+1.30 (*vs.* RHE)	390 (*vs.* RHE)	-	[214]
Pb-Bi	-	4.79 M H_2SO_4	-	Melted/casted	7.33% Bi	+1.40 (*vs.* Hg_2SO_4/Hg)	290 (*vs.* Hg_2SO_4/Hg)	-	[215]
Ti-MnO_2	GC	0.05 M H_2SO_4	1 $mAcm^{-2}$ loss after 2h at 1.9 V (*vs.* RHE)	Drop casting	-	+1.60 (*vs.* RHE)	-	-	[140]
MnO_2	GC	0.05 M H_2SO_4	1 $mAcm^{-2}$ loss after 2h at 1.9 V (*vs.* RHE)	Drop casting	-	+1.61 (*vs.* RHE)	-	170	[140]
MnO_x	FTO	0.5 M H_2SO_4	18% Mn dissolution after 1h at pH 2	Electrodeposition	6 mC/cm^2	+1.47 (*vs.* RHE)	-	60.3	[135]
Co_3O_4	FTO	0.5 M H_2SO_4	12h at 10 $mAcm^{-2}$	Spin casting	200 µL	+1.63 (*vs.* RHE)		-	[216]
$CoMnO_x$	FTO	100 mM Phosphate & 1 M KNO_3 (pH 2.5)	30 mins at 1 $mAcm^{-2}$	Electrodeposition	0.5 mM	*ca.* +1.70 (*vs.* NHE)	-	~83	[142]

CoO_x	FTO	100 mM Phosphate & 1 M KNO_3 (pH 2.5)	20 mins at 1 $mAcm^{-2}$	Electrodeposition	0.5 mM	*ca.* +1.70 (*vs.* NHE)	-	82	[142]
$CoPbO_x$	FTO	100 mM Phosphate & 1 M KNO_3 (pH 2.5)	7h at 1 $mAcm^{-2}$	Electrodeposition	0.5 mM	*ca.* +1.65 (*vs.* NHE)	-	~72	[142]
$CoFePbO_x$	FTO	100 mM Phosphate & 1 M KNO_3 (pH 2.5)	>50h at 1 $mAcm^{-2}$	Electrodeposition	0.5 mM	*ca.* +1.65 (*vs.* NHE)	-	~70	[142]
FeO_x	FTO	100 mM Phosphate & 1 M KNO_3 (pH 2.5)	2h at 1 $mAcm^{-2}$	Electrodeposition	0.5 mM	-	-	51	[142]
MnO_x	FTO	100 mM Phosphate & 1 M KNO_3 (pH 2.5)	10 mins at 1 $mAcm^{-2}$	Electrodeposition	0.5 mM	*ca.* +2.40 (*vs.* NHE)	-	650	[142]
PbO_x	FTO	100 mM Phosphate & 1 M KNO_3 (pH 2.5)	12h at 1 $mAcm^{-2}$	Electrodeposition	0.5 mM	-	-	121	[142]
NiO_x	FTO	100 mM Phosphate & 1 M KNO_3 (pH 2.5)	-	Electrodeposition	0.5 mM	*ca.* +1.60 (*vs.* NHE)	-	N/A	[142]
NiO_x	GC	1 M H_2SO_4	Unstable in acid	Electrodeposition	40 mL	-	~1200 (*vs.* SCE)	-	[126]
$NiCuO_x$	GC	1 M H_2SO_4	Unstable in acid	Electrodeposition	40 mL	-	~1210 (*vs.* SCE)	-	[126]
$NiCoO_x$	GC	1 M H_2SO_4	Unstable in acid	Electrodeposition	40 mL	-	~1000 (*vs.* SCE)	-	[126]
$NiFeO_x$	GC	1 M H_2SO_4	Unstable in acid	Electrodeposition	40 mL	-	~1000 (*vs.* SCE)	-	[126]
CoO_x	GC	1 M H_2SO_4	Unstable in acid	Electrodeposition	40 mL	-	~1000 (*vs.* SCE)	-	[126]
$CoFeO_x$	GC	1 M H_2SO_4	Unstable in acid	Electrodeposition	40 mL	-	~700 (*vs.* SCE)	-	[126]
CoP_i	GC	1 M H_2SO_4	Unstable in acid	Electrodeposition	40 mL	-	~700 (*vs.* SCE)	-	[126]

$MnSb_{1.7}O_y$	ATO film on quartz	1 M H_2SO_4	>144h at 10 $mAcm^{-2}$	Magnetron sputtering	-	+1.78 (*vs.* RHE)	670 (*vs.* RHE)	96	[151]
$Ni_{0.2}Mn_{0.8}Sb_{1.6}O_y$	ATO film on quartz	1 M H_2SO_4	>144h at 10 $mAcm^{-2}$	Magnetron sputtering	-	+1.70 (vs. RHE)	690 (*vs.* RHE)	60	[151]
$NiSb_{1.8}O_y$	ATO film on quartz	1 M H_2SO_4	>144h at 10 $mAcm^{-2}$	Magnetron sputtering	-	+1.80 (*vs.* RHE)	1000 (*vs.* RHE)	105	[151]
1T MoS_2	CFP	0.5 M H_2SO_4	1h at 10 $mAcm^{-2}$	Spray deposition	-	*ca.* +1.50 (*vs.* RHE)	420 (*vs.* RHE)	322	[155]
1T TaS_2	CFP	0.5 M H_2SO_4	1h at 10 $mAcm^{-2}$	Spray deposition	-	*ca.* +1.60 (*vs.* RHE)	450 (*vs.* RHE)	282	[155]
2H MoS_2	CFP	0.5 M H_2SO_4	1h at 10 $mAcm^{-2}$	Spray deposition	-	*ca.* +1.60 (*vs.* RHE)	480 (*vs.* RHE)	361	[155]
2H TaS_2	CFP	0.5 M H_2SO_4	1h at 10 $mAcm^{-2}$	Spray deposition	-	*ca.* +1.70 (*vs.* RHE)	540 (*vs.* RHE)	265	[155]
$Cu_{1.5}Mn_{1.5}O_4$	Ti foil	0.5 M H_2SO_4	-	Drop casting	-	*ca.* +1.43 (*vs.* RHE)	310 (*vs.* RHE)	-	[144]
$Cu_{1.5}Mn_{1.5}O_4$:F	Ti foil	0.5 M H_2SO_4	24h at 16 $mAcm^{-2}$	Drop casting	-	*ca.* +1.43(*vs.* RHE)	320 (*vs.* RHE)	-	[144]

Key: PCP; Porous carbon polyhedron NrGO; Nitrogen doped reduced graphene oxide NC; Nanocage NW: Nanowire NRA; Nanorod array NF; Nickel foam MWCNTS; Multiwalled carbon nanotubes NMCC; Nitrogen doped mesoporous carbon cage CFP; Carbon filter paper BCCF; Bacterial cellulose carbon fibers GCNS; Graphene carbon nanosheets